Article:
González-Novo, R., Zamora-Carreras, H., Armesto, M. et al. (2026) 3D environment favors persistent changes in cell functions and altered morphology, wrinkling, and biomechanical signature of the nucleus. Cell Reports Physical Science, 7 (2). 103116. ISSN: 2666-3864

https://doi.org/10.1016/j.xcrp.2026.103116

Cell Reports
Physical Science

Article

3D environment favors persistent changes in cell functions and altered morphology, wrinkling, and biomechanical signature of the nucleus

Graphical abstract

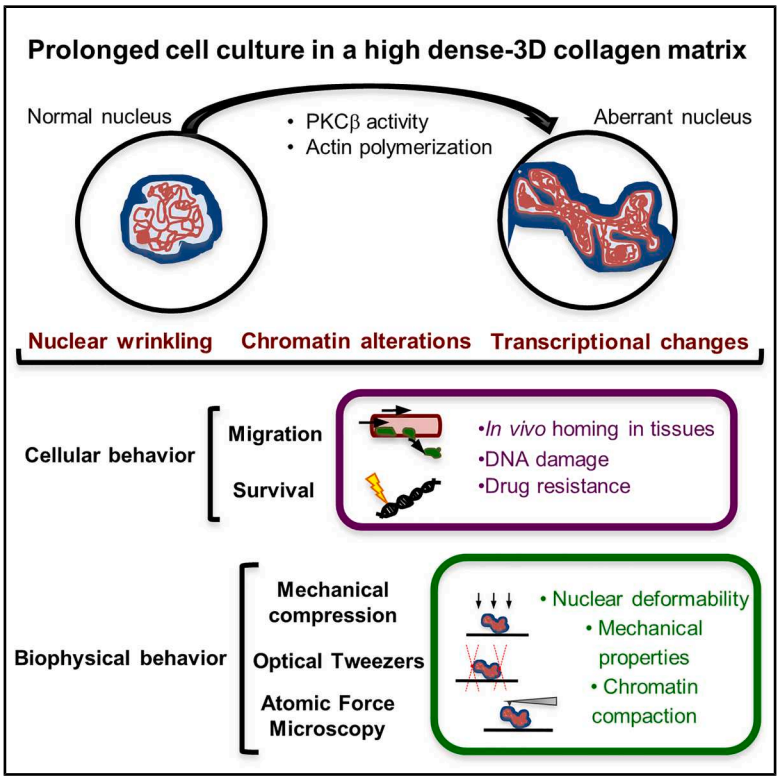

Highlights

- 3D confinement induces persistent nuclear changes in transformed (TR) leukemia cells
- Lamin B1 staining reflects nuclear wrinkling and altered actin and PKCβ signaling of TR cells
- TR cells show altered transcriptional activity, chromatin organization, and cellular functions
- Nuclear changes of TR cells display a distinct and homogeneous biomechanical signature

Authors

Raquel González-Novo, Héctor Zamora-Carreras, Marina Armesto, ..., Lin Wang, Christopher P. Toseland, Javier Redondo-Muñoz

Correspondence

javier.redondo@cib.csic.es

In brief

González-Novo et al. show that 3D microenvironments drive persistent chromatin, morphological, and mechanical remodeling of the leukemia cell nucleus. These nuclear changes alter transcription, survival, and *in vivo* dissemination, revealing how 3D matrix confinement might reshape leukemia cell biology.

González-Novo et al., 2026, Cell Reports Physical Science *7*, 103116
February 18, 2026
https://doi.org/10.1016/j.xcrp.2026.103116

CellPress

Cell Reports
Physical Science

CellPress
OPEN ACCESS

Article

3D environment favors persistent changes in cell functions and altered morphology, wrinkling, and biomechanical signature of the nucleus

Raquel González-Novo,[1] Héctor Zamora-Carreras,[1] Marina Armesto,[1] Ana de Lope-Planelles,[1] Horacio López-Menéndez,[2,3] Pedro Roda-Navarro,[4] Francisco Monroy,[2,3] Lin Wang,[5] Christopher P. Toseland,[6] and Javier Redondo-Muñoz[1,7,*]

[1]Department of Biomedicine, Centro de Investigaciones Biológicas Margarita Salas, 28040 Madrid, Spain
[2]Department of Physical Chemistry, Complutense University, 28040 Madrid, Spain
[3]Translational Biophysics, Hospital Doce de Octubre Health Research Institute (imas12), 28041 Madrid, Spain
[4]Department of Immunology, School of Medicine, University Complutense de Madrid and Doce de Octubre Health Research Institute (imas12), 28040 Madrid, Spain
[5]Central Laser Facility, Research Complex at Harwell, Science and Technology Facilities Council, Rutherford Appleton Laboratory, Harwell, Oxford OX11 0QX, UK
[6]Division of Clinical Medicine, School of Medicine and Population Health, University of Sheffield, Sheffield S10 2RX, UK
[7]Lead contact
*Correspondence: javier.redondo@cib.csic.es
https://doi.org/10.1016/j.xcrp.2026.103116

SUMMARY

The interplay between cells and their surrounding microenvironment drives multiple cellular functions, including migration, proliferation, and cell fate transitions. The nucleus is a mechanosensitive organelle; however, the morphological and functional changes of the nucleus induced by a three-dimensional (3D) extracellular environment remain unclear. Here, we report that leukemia Jurkat cells selected after 3D growth conditions retain persistent nuclear changes even after being released from confinement. These altered cells showed aberrant nuclear wrinkling, visualized by the lamin B1 distribution and mediated by disrupted actin dynamics and protein kinase C (PKC)β signaling. Moreover, these cells presented changes in chromatin compaction, transcription, apoptosis, and *in vivo* dissemination. By combining biomechanical techniques and single-nucleus analysis, we have determined that these cells exhibit a distinct nuclear mechanical behavior and biophysical signature compared with control cells. Together, these findings demonstrate that 3D microenvironments alter leukemia cell biology by promoting persistent changes in chromatin organization, morphology, and mechanical response of the nucleus.

INTRODUCTION

The cell nucleus is organized into the nuclear envelope and the underlying lamina network, which encloses chromatin and controls multiple DNA functions.[1,2] In the physiological context, cells have to respond to external stimuli, including biochemical signals, but also biomechanical properties of the extracellular microenvironment.[3,4] The mechanical response of the nucleus is dictated by the chromatin and the lamina network,[5] which, in turn, is critical in multiple processes, including altered gene expression, cell fate transitions, cell migration, cell cycle progression, and tumorigenesis.[6,7] Multiple biophysical techniques have been used to characterize the nuclear mechanical changes, such as cell stretching, substrate patterning, external compression, and three-dimensional (3D) cell migration.[8–10] Interestingly, studying the behavior of the nucleus in intact cells might lead to misinterpretation due to the cell membrane and the cytoskeleton; thereby, an integral study of intact cells and isolated nuclei might bypass this issue to better define the biophysical changes interpreted by the nucleus.[11] This is particularly important from basic and translational research, as alterations in the deformability of the nucleus induced by the extracellular matrix (ECM) have been described in multiple human pathologies, including inflammation, aging, and cancer.[12–14]

The ECM provides mechanical and chemical signals that regulate cellular functions (such as cell migration, apoptosis, and differentiation) and phenotypical changes.[15] Notably, in 3D environments, cells are confined by the surrounding ECM that promotes specific intracellular signals.[16] It has been previously shown that *in vitro* 3D confinement compromises nuclear stability, promotes nuclear rupture and DNA damage, and perturbs different functions, such as DNA repair, cell differentiation, and histone methylation.[17–20] Moreover, these alterations have been linked to larger physiological processes related to metabolism, mitochondrial activity, senescence, and drug resistance.[21,22] Despite this evidence, it is not yet known how cell-environment interactions impact alterations in the nucleus that drive genomic instability and cancer progression.

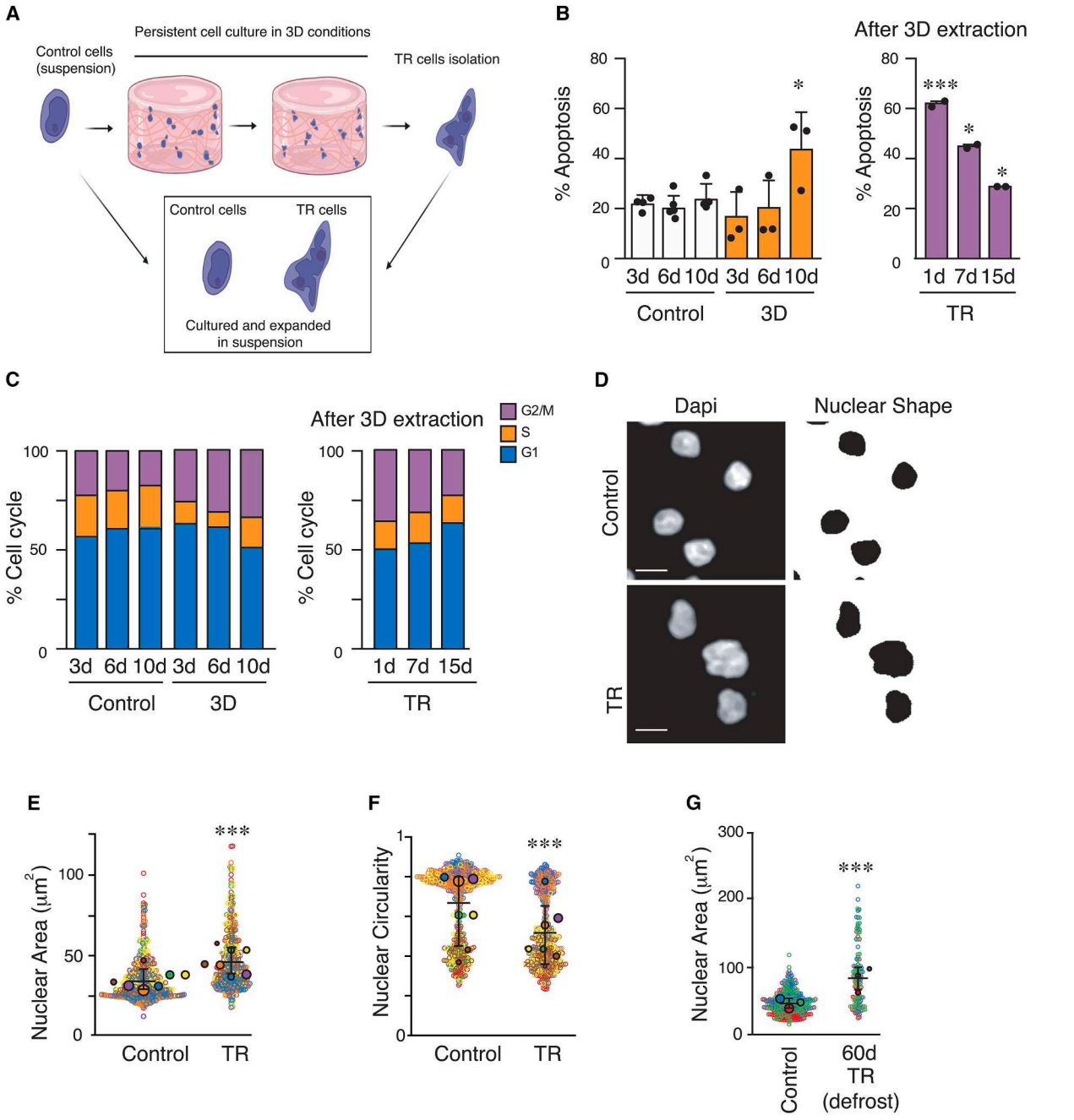

Figure 1. 3D cell confinement promotes persistent morphological changes in the nucleus

(A) Jurkat cells were embedded in a 3D collagen matrix (3.3 mg/mL) in complete medium and maintained in culture for 10 days. Then, the collagen gel was disaggregated mechanically, and transformed (TR) cells were collected, kept in suspension without any further constriction, and expanded as TR cells. Control and TR cells were cultured in suspension, expanded, and used for experimental procedures.

(B) Cells were cultured in suspension (control) or in 3D collagen matrices (3.3 mg/mL) for 3, 6, and 10 days. Additionally, cells cultured for 10 days, defined as TR, were extracted from the collagen and cultured in suspension for the indicated days. Then, cells were collected and apoptosis analyzed by flow cytometry. $n = 3$ replicates ±SD.

(C) Cells cultured as in (B) were collected, fixed, permeabilized, and stained with propidium iodide. Then, cell cycle progression was analyzed by flow cytometry with G1, S, and G2/M phases depicted according to DNA content. $n = 3$ replicates ± SD.

(D) Control and TR cells were sedimented on poly-L-lysine-coated coverslips, fixed, and stained with Hoechst for analysis by confocal microscopy. The images on the right indicate the shape of the nuclei in black. Bar: 10 μm.

(legend continued on next page)

Here, we described how cell confinement causes a selection of cells presenting persistent changes that influence the mechanical and functional responses. We focused on Jurkat cells for their well-characterized responses to mechanical stimuli. We cultured cells embedded in a high-density 3D collagen I matrix for several days and then collected and cultured them in suspension as TR (transformed) cells, which present persistent functional and phenotypical changes due to the memory of 3D confinement. In terms of morphological and phenotypical changes, we demonstrated that highly confining 3D conditions, which mimic the dense extracellular environments encountered *in vivo*, induced an increment and wrinkling of the nucleus and lamin B1. Moreover, we observed that actin polymerization and protein kinase C (PKC) activity might be linked to the nuclear phenotype and lamin B1 visualization of TR cells. Our transcriptional analysis reveals that TR cells showed a different transcriptional activity and state compared to control cells, indicating potential differences between short-term cellular responses and the mechanical adaptation to 3D environments. Importantly, we revealed that 3D confinement affected the biology of TR cells in functions such as survival and *in vivo* dissemination. Finally, we combined atomic force microscopy (AFM), super-resolution microscopy, confined compression, and optical tweezers to demonstrate that TR cells showed a homogeneous biomechanical signature inside the nucleus coupled to the redistribution of chromatin. Our results reinforce the idea that the ECM and the microenvironment can drive nuclear changes, which may influence transcriptional activity, biomechanical signatures, and functional differences, although extensive research will be essential to establish broader biological relevance.

RESULTS

Leukemia cells display morphological changes in the nucleus due to mechanical adaptation after 3D conditioning

Collagen is the most abundant ECM scaffolding protein, and collagen matrices have been extensively used as a physiological model of physical barriers to study the migration and plasticity of normal and tumor cells.[23–26] Furthermore, the adaptation of cells to ECM stiffness is critical for multiple homeostatic and pathological conditions *in vivo*.[27,28] To investigate how the mechanical signals from the ECM might promote the adaptation of cancer cells, we designed a workflow to select leukemia cells collected after 3D confinement in a collagen I gel. The cells were compared to the starting population of cells, which had never undergone 3D mechanical confinement (Figure 1A).

First, we evaluated the behavior of leukemia cells surrounded by high-density collagen (3.3 mg/mL) over time, which might promote mechanical stress. To understand how the 3D collagen matrix might affect the survival and proliferation of leukemia cells, we compared cells in suspension (control), cells cultured in 3D confinement for several days, and the survivor cells after 10 days (referred to as TR cells). We observed that the mechanical stress induced by 3D confinement increased the apoptosis of leukemia cells; nonetheless, survivor TR cells progressively recovered their viability in the absence of confinement (Figure 1B). We observed only slight differences in the cell cycle progression after culturing leukemia cells in 3D conditions (Figure 1C). Similar to cell viability, we confirmed a reduction in the proliferative ratio of leukemia cells induced by 3D confinement (Figure S1).

The nucleus plays a critical role during the cell invasion into the 3D ECM and in tumor dissemination during the metastasis process,[29] and alterations in its size and morphology serve as a marker in human pathologies, such as cancer.[30] First, we visualized the nuclear morphology of control and TR cells (Figure 1D). We used a linear mixed-effects model to assess differences in nuclear area between control and TR cells, with condition as a fixed effect and experiment as a random intercept (REML estimation and variance components structure), and found that TR cells showed bigger nuclei with a diminished circularity than their counterparts (Figures 1E and 1F). In addition to confocal analysis, the size and complexity of cells and nuclei can be determined by flow cytometry,[31] and we have confirmed that the isolated nuclei distributed from TR cells have a larger size and more complexity, suggesting more irregular shapes, than those from control cells (Figure S1). To further study the nuclear morphology, we visualized control and TR cells by electron microscopy (EM) and confirmed that TR cells showed an aberrant nuclear shape compared to control cells (Figure S1). We confirmed that TR cells remained distinct from control cells even after freeze-thaw cycles (Figure 1G), suggesting that this time window was sufficient for subsequent functional and morphological characterization.

As EM images also suggested differences in the nucleolar disposition of TR cells (Figure S1), we stained control and TR cells for nucleolin. Remarkably, we confirmed a significant increment in the intensity of the signal and the nucleolar area of TR cells (Figure S1). Together, our results showed the possibility of selecting and expanding an altered leukemia subtype showing nuclear morphological changes and a persistent adaptation to the mechanical stress to 3D confinement, which serves, together with the original population (control), as an ideal cell model to study cellular adaptation to 3D confinements.

Cells derived after 3D mechanoadaptation present higher basal DNA damage levels and susceptibility to apoptosis

Confined conditions regulate the proliferation and cell cycle progression of cells.[32,33] First, we investigated whether TR cells showed alterations in their proliferative ratio and found no significant differences in the proliferation of control and TR cells (Figure 2A). We stained Ki67 and the BrdU (bromodeoxyuridine) incorporation in control and TR cells growing exponentially and

(E and F) Changes in the nuclear area (E) and circularity (F) of control and TR cells. Each point represents a single cell, color coded by experimental replicate. Big dots show the mean value per experiment, and their size is proportional to the n of the corresponding experiment. $n = 7$ replicates, $N = 459–580$ cells ± SD.
(G) Control and TR cells after defrosting at 60 days were seeded onto poly-L-lysine-coated slides, fixed, and stained with Hoechst for analysis by confocal microscopy. Each point represents a single cell, color coded by experimental replicate. Big dots show the mean value per experiment, and their size is proportional to the N of the corresponding experiment. $n = 3$ replicates, $N = 135–406$ cells ± SD. $^{*}p < 0.05$ and $^{***}p < 0.001$.

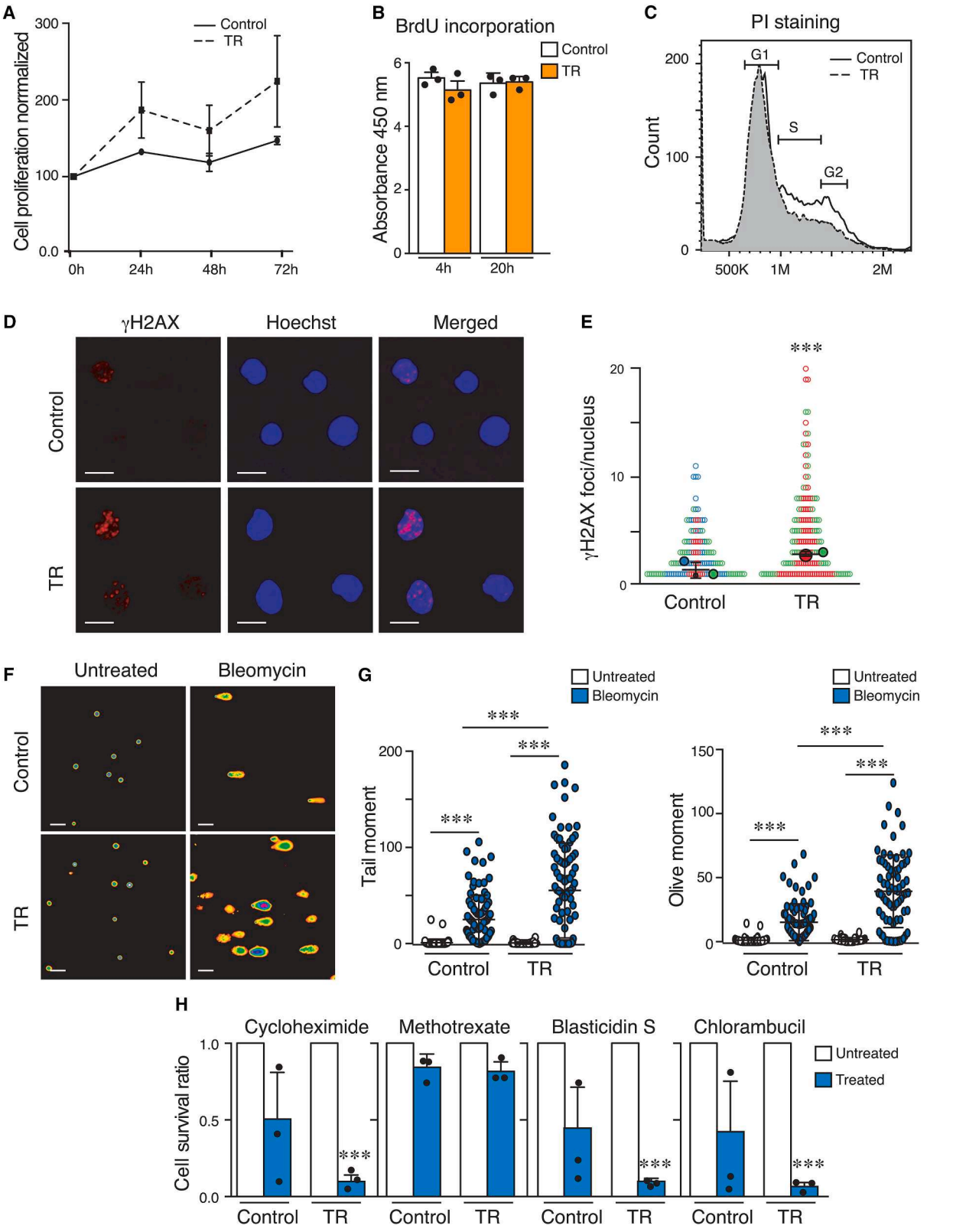

(legend on next page)

found similar levels of these proliferative markers in both cell types (Figures 2B and S2). We confirmed that control and TR cells showed similar cell cycle profiles, without a significant increment in the population showing a higher DNA amount (Figure 2C). Moreover, we analyzed the presence of polyploid species in control and TR cells and confirmed no significant changes in the amount of DNA or the presence of hyperploidy in TR cells (Figure S2), indicating that TR cells display an aberrant nuclear morphology without affecting the polyploidy. We tested the expression of cyclins and observed that TR cells exhibited a slight reduction of cyclin A (a typical cyclin for late phases of the cell cycle) compared to control cells (Figure S2).

Cell migration through confined spaces compromises nuclear integrity and promotes DNA damage, including the marker phospho-histone γH2AX.[34] We found that nuclei of TR cells showed more foci of γH2AX per nucleus than control cells (Figures 2D and 2E). We further confirmed these results by measuring the total levels of γH2AX in control and TR cells (Figure S3) and by quantifying other DNA damage markers, such as phospho-ATM (pATM) (Figure S3). As we found high levels of DNA damage markers in TR cells, we characterized their DNA repair response by treating control and TR cells with bleomycin, a drug that induces DNA damage. We visualized the levels of DNA damage by single-cell electrophoresis (comet assay) and found that TR cells were more sensitive to DNA damage than control cells (Figures 2F, 2G, and S3). Moreover, given the potential implication of the basal levels of DNA damage response (DDR) on the survival capacity of the cells, we tested whether TR cells were more sensitive to conventional chemotherapies than control cells. Interestingly, we confirmed that TR cells showed more sensitivity to cell death in response to several chemotherapeutic drugs than control cells (Figures 2H and S3). Together, our results suggest that mechanoadapted TR cells alter their response to DNA damage.

Derived cells after 3D mechanoadaptation reduce their *in vivo* invasiveness

Nuclear adaptation is critical during cell migration through physical barriers such as the endothelium and the interstitial spaces,[26,35,36] and we evaluated whether the mechanical adaptation of TR cells might alter other functions, such as cell migration. Firstly, we performed a chemotaxis assay and found that TR cells did not show significant differences in their chemotactic response to serum (Figures 3A and S4). To discount defective cell adhesion, we evaluated how control and TR cells attach to VCAM-1 (vascular adhesive molecule-1), and we found similar levels of cell adhesion for control and TR cells (Figure S4). We also tested whether TR cells present spreading defects on 2D surfaces with non-specific ligands and found no differences in the cell adhesion kinetics of control and TR cells at short times, while a shrinking of the cell area in control cells could be observed after 2 h (Figures 3B and 3C). Similar results were observed on collagen- and VCAM-1-coated surfaces, which offer a more physiological context, showing that control and TR cells spread similarly (Figure S4). Importantly, we confirmed that cell culture on the 2D-collagen surface did not promote nuclear wrinkling or alterations (Figure S4). To further determine the migration behavior of TR cells *in vitro*, we analyzed their capacity to infiltrate a collagen matrix and found that the invasion depth of TR cells was not impaired (Figures 3D and 3E). The mechanoadaptation of solid tumors favors the malignant metastatic phenotype[21]; therefore, although we did not see differences *in vitro*, we assessed how TR cells might have altered their invasive capacity *in vivo*. For this, we injected an equal number of control and TR cells labeled with vital dyes into the tail vein of immunodeficient recipient mice and analyzed the homing of cells into the bone marrow, liver, and spleen at 24 h post-injection. Our analysis indicated a reduction of TR cells reaching these organs compared to controls (Figures 3F and S4), independently of the vital dye used (Figure S4). Together, these results indicate that TR cells derived after 3D confinement exhibit less capacity to invade tissues *in vivo* without affecting their chemotaxis or cell adhesion.

Derived cells after 3D mechanoadaptation show transcriptional changes

It was recently published that ECM density promotes cell fate transition in fibroblasts,[37] and we interrogated the transcriptomic changes induced in TR cells. We isolated the mRNA from control and TR cells cultured in suspension and exponential growth and then analyzed them by microarray expression. Our analysis showed a significant differential expression (1.4-fold change, adjusted $p < 0.05$, and $|\log2 \text{ fold change}| > 0.5$) for 661 genes (143 up- and 518 downregulated) in TR cells compared with control cells (Figures 4A and 4B). To focus on the effect of mechanical adaptation induced in TR cells after 3D confinement, we

Figure 2. TR cells from persistent 3D confinement show alterations in their survival response

(A) Control or TR (dark and dashed lines, respectively) cells were cultured, and proliferation was quantified by MTT assay at the indicated times. Mean $n = 5$ replicates ± SD.

(B) Control and TR cells were incubated with 5-bromo-2′-deoxyuridine (BrdU) for 4 and 20 h. Then, cells were fixed, and BrdU incorporation was quantified. Mean $n = 3$ replicates ± SD.

(C) Control (white) and TR (gray, dashed line) cells were fixed, permeabilized, and stained with propidium iodide. Then, cell cycle progression was analyzed by flow cytometry. G1, S, and G2/M phases are shown according to DNA content.

(D) Control and TR cells were collected, seeded onto poly-L-lysine-coated slides, fixed, and stained for γH2AX (red) and Hoechst (blue). Bar: 10 μm.

(E) Number of foci per nucleus of control or TR cells. Each point represents a single cell, color coded by experimental replicate. Big dots show the mean value per experiment, and their size is proportional to the n of the corresponding experiment. $n = 2$ replicates, $N = 247–252$.

(F) Control and TR cells were treated with 40 μM bleomycin for 4 h, embedded in agarose, and lysed. An alkaline comet assay by electrophoresis was performed to visualize DNA by fluorescence microscopy. Bar: 40 μm.

(G) Tail and olive moment analysis of the comet assay in (F). $n = 7$ replicates, $N = 58–85$ cells ± SD.

(H) Control and TR cells were cultured in the presence of the indicated drugs (1 μM methotrexate, 5 μg/mL cycloheximide, 5 μg/mL blasticidin S, or 10 μg/mL chlorambucil) for 24 h. Then, cells were collected and stained for annexin V-FITC and propidium iodide for flow cytometry analysis. The survival ratio of control and TR cells upon normalization to their untreated conditions is shown. Mean $n = 3$ replicates ± SD. $^{***}p < 0.001$.

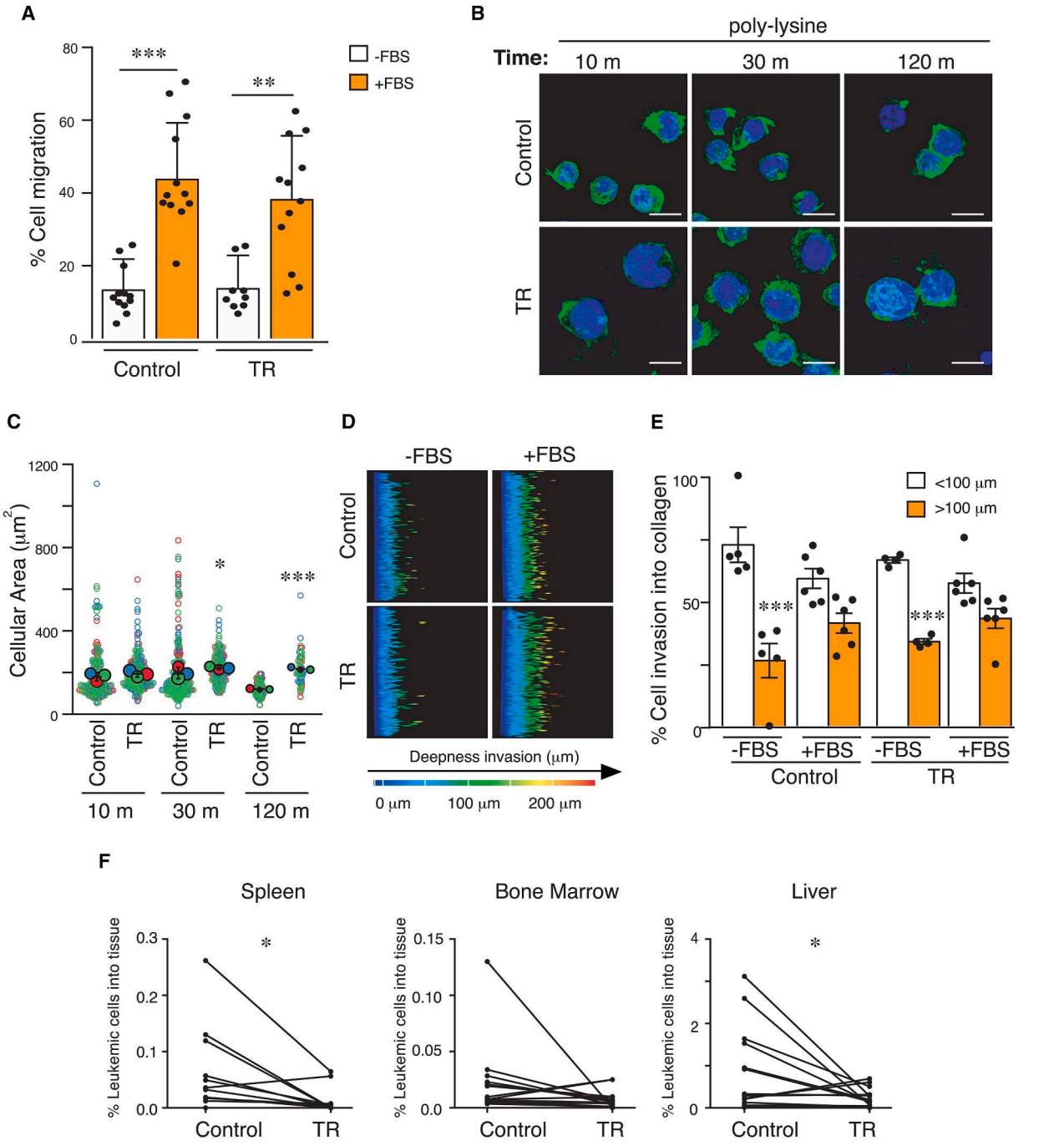

Figure 3. Aberrant cells after suffering 3D confinement exhibit reduced cell invasiveness

(A) Control and TR cells were seeded on the top chamber of Transwell inserts and allowed to migrate through 5 μm pores toward FBS for 24 h. The graph shows the percentage of migrated cells. Mean *n* = 12 replicates ± SD.

(B) Control and TR cells were seeded on poly-L-lysine-coated slides, fixed at the indicated times, and stained with phalloidin (green) and Hoechst (blue). Bar: 10 μm.

(C) Cellular area analysis of the adhesion kinetics in (B). Each point represents a single cell, color coded by experimental replicate. Big dots show the mean value per experiment, and their size is proportional to the *n* of the corresponding experiment. *n* = 3 replicates *N* = 55–256 cells ± SD.

(D) Control and TR cells were seeded on the top of a collagen 3D matrix and cultured at 37°C for 24 h. Then, cells were fixed and stained with propidium iodide, and serial confocal images of the matrix were taken to calculate the invasion depth of control and TR cells toward FBS.

(legend continued on next page)

performed bioinformatics analysis of the gene expression profiles and found that the most significant changes correspond to genes encoding mitochondrial transport, cytokine signaling, and ECM organization pathways (Figures 4C and S5; Table S1). To validate our data, we selected MEN1 and EHMT2 (corresponding to the protein G9a, a histone methyltransferase involved in H3K9 methylation and leukemia progression),[38,39] and determined their levels by RT-qPCR. Consistent with our transcriptional analysis, we found a reduced level of both genes in TR cells (Figure S5). We subsequently performed a transcriptional analysis of leukemia cells following short-term embedding in 3D confinement to investigate whether the altered genes observed in TR cells corresponded to a mechanoadaptation after prolonged 3D confinement or if it also occurred at shorter timescales. For this, we cultured cells in suspension or embedded them in a 3D collagen matrix for 3 h, which has been reported to induce H3K4 methylation in leukocytes[18] (Figures 4D and 4E; Table S2). We found only 38 common genes altered in cells cultured for 3 h in 3D confinement and in TR cells; some of them are particularly relevant for tumorigenic processes (Figure S5; Table S3), indicating that mechanoadapted TR cells showed different outputs in cell biology than cells suffering 3D confinement for short-term conditions.

Next, we interrogated whether the TR cells' altered gene expression profile might reflect different transcriptional activity compared to control cells. We measured the levels of RNA polymerase II (RNA pol II) and the incorporation of an alkyne-modified nucleoside, 5-ethynyl uridine (EU), and found that TR cells showed increased levels of RNA Pol II compared to control cells (Figures 4F, 4G, and S5). We also observed an increment of EU incorporation in TR cells by flow cytometry (Figure S5). We confirmed the correlation between RNA Pol II levels and transcription activity, although control cells showed lower levels of these signals compared to the broad scatter in TR cells (Figure S5). To further confirm the activation of RNA Pol II, we measured the levels of RNA Pol II phosphorylation and found that TR cells showed increased levels of phospho-RNA Pol II (Figures 4H, 4I, and S5). Together, these results denote that TR cells exhibit enduring transcriptional changes after their mechanoadaptation in 3D environments.

Lamin B1 staining reveals a multilobular disposition of the nucleus in cells derived after 3D mechanoadaptation

In contrast to adherent cells, where A-type lamins are the major component of the nuclear lamina, leukocytes mainly express lamin B.[40] Since dense 3D collagen matrix alters the size and morphology of TR cells, we hypothesized that lamin B1 distribution may also be affected in these cells. First, we visualized the nucleus of control and TR cells and found that lamin B1 localized in the nuclear periphery of control cells, while TR cells presented an irregular distribution of this protein at the periphery but also in the central part of the nucleus (Figures 5A–5C). To distinguish whether aberrant lamin B1 visualization corresponded to intranuclear localization or to nuclear surface wrinkling, we characterized differences in the morphology and lamin B1 distribution of nuclei from control and TR cells by performing 3D reconstruction (Videos S1 and S2). We observed aberrant lamin B1 wrinkles in the middle cross-section plane of TR cells (Figure 5D), indicating that TR cells presented alterations in nuclear morphology, which may reflect a redistribution of nuclear dimensions and increased nuclear volume. To confirm these results, we performed staining of the nuclear envelope marker, emerin, and found that most of the emerin signal also localized at the nuclear wrinkles, suggesting that the reshaping of the nucleus reflects wrinkling and not soluble lamin detached from the nuclear envelope (Videos S3 and S4; Figure 5E). We evaluated changes in the expression of nuclear envelope proteins in TR cells and found that TR cells showed no significant changes in the levels of emerin and sun2 proteins (Figure S6). To identify how the 3D confinement of the ECM might affect lamin B1 distribution in leukemia cells, we evaluated the nuclear morphology and lamin B1 visualization after cell confinement in a 3D collagen gel and found that 3 days was sufficient to promote the irregular distribution of lamin B1 and an increase in nuclear size (Figure S6). Lamin B interacts and regulates nucleolar components[41–43]; therefore, we interrogated whether the aberrant distribution of lamin B1 in TR cells might regulate its interaction with nucleolar proteins. First, immunoprecipitation experiments revealed that TR cells presented similar levels of lamin B1 bound to the nucleolar protein NPM1 as control cells (Figure S6). As expected, the disposition of nucleoli in TR cells was not connected to the abnormal distribution of lamin B1 (Figure S6). These results indicate that TR cells showed an aberrant localization of lamin B1 in a multilobular shape.

PKC activity and actin polymerization modulate the phenotypical visualization of lamin B1 in cells derived after 3D mechanoadaptation

It is well known that lamin B1 is regulated by multiple kinases.[44] We selectively inhibited conventional PKC activity with staurosporine (for PKCα) and enzastaurin (for PKCβ) and found no significant differences in the visualization of lamin B1 (Figure S7). To further determine the possible role of PKC, we transfected TR cells with a specific pool of small interfering RNAs (siRNAs) against PKCβ (Figure S7) and found that TR cells depleted for PKCβ recovered the signal of lamin B1 at the nuclear periphery and the rounded phenotype of the nucleus (Figures 6A, 6B, and S7). As we have previously described that PKCβ localizes mainly in the nucleus of leukemia cells,[39] we observed increased basal levels of phospho-PKC in the nuclear and chromatin fractions of PKC in TR cells (Figures 6C and S7). The cytoskeleton mediates mechanical signals between cells and their surrounding environment.[45] We addressed the potential implication of actin polymerization on the phenotypic visualization of lamin B1 in TR cells. For this, we incubated TR cells with drugs to target actin polymerization and found that cells treated for 1 h with latrunculin B (an actin polymerization inhibitor) recovered lamin

(E) Percentage of cells invading into the collagen gel deeper than 100 μm. Mean $n = 4$ replicates ± SD.
(F) Control (Far Red+) and TR (CFSE+) cells were stained with live-cell dyes, mixed 1:1, and injected into the tail vein of NSG (NOD scid gamma mouse) mice. After 24 h, the percentage of infiltrated leukemic cells according to the total number of events into the spleen, bone marrow, and liver for each animal was determined by flow cytometry. $n = 14$. $^{*}p < 0.05$, $^{**}p < 0.01$, and $^{***}p < 0.001$.

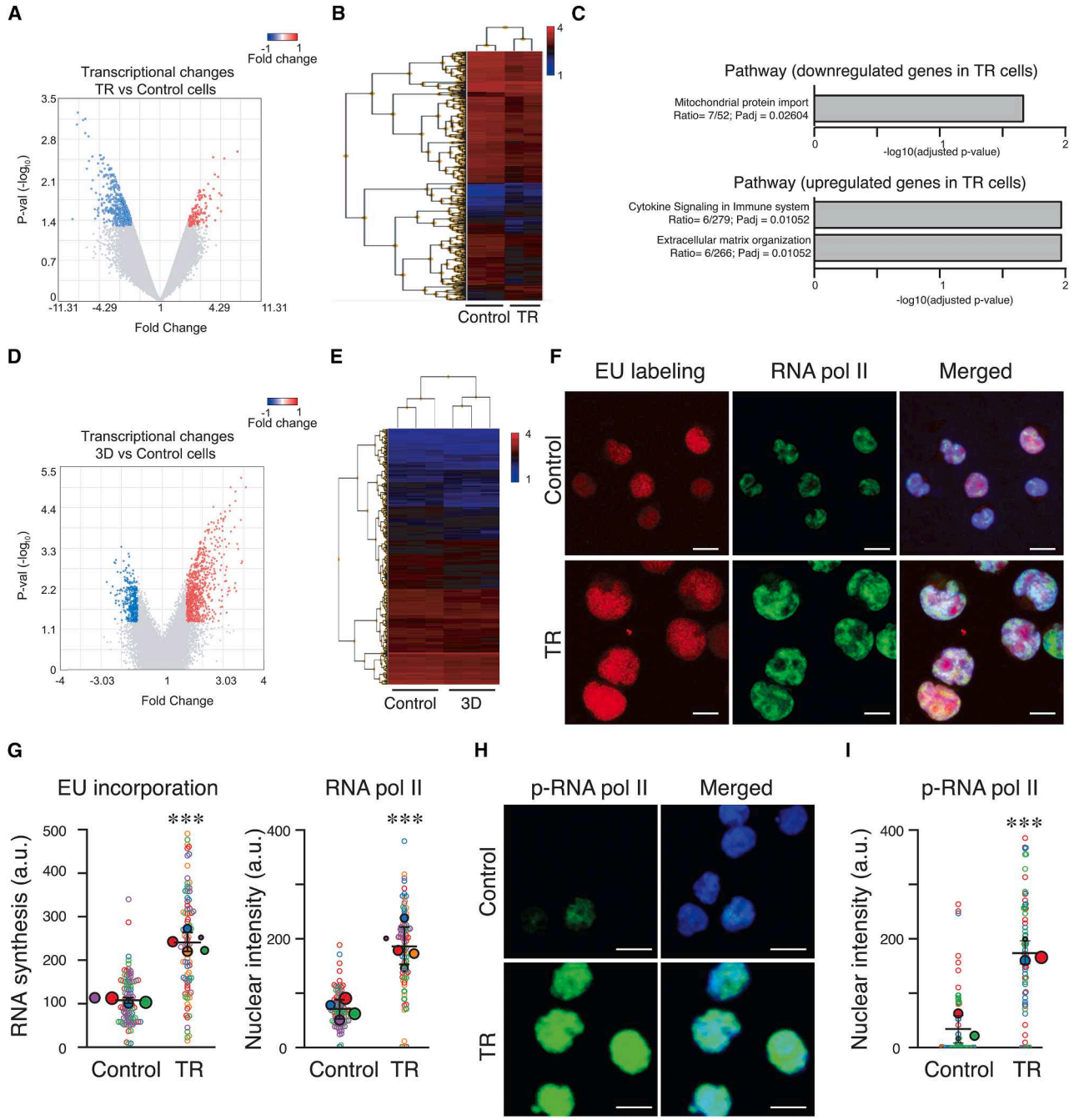

Figure 4. TR cells from 3D confinement alter their transcriptional program

(A) Control or TR cells in exponential growth were lysed, mRNA was isolated, and transcriptional changes were analyzed by mRNA expression microarray. Volcano plot shows significantly downregulated (blue) and upregulated (red) transcripts in TR cells compared to control conditions. The graph shows the double filtering criterion |fold change| > 1.4 and $p < 0.05$ ($n = 2$ replicates); all other genes that were not found to be significantly altered are shown as gray dots.

(B) Heatmap of the relative gene expression patterns generated from the microarray data in (A), reflecting log2 normalized gene expression values. The color scale illustrates the relative expression level of genes across all samples from a red color (higher expression) to a blue color (lower expression).

(C) Pathway enrichment analysis based on differentially up- and downregulated genes in control compared with TR Jurkat cells.

(D) Jurkat cells were cultured in suspension (control) or embedded in a 3D collagen type I matrix for 3 h (3D). Cells were collected and lysed, and mRNA was extracted for the analysis of transcriptional changes by microarray. A volcano plot was generated by double filtering criterion |fold change| > 1.4 and $p < 0.05$ ($n = 2$ replicates). Blue and red dots show the downregulated and upregulated transcripts, respectively. All other genes that were not found to be significantly altered are shown as gray dots.

(legend continued on next page)

B1 at the nuclear periphery of TR cells, while jasplakinolide, which stabilizes polymerized actin, did not significantly alter the distribution of lamin B1 (Figures 6D and 6E).

It has been reported that nuclear actin and its associated proteins play fundamental nuclear functions, such as chromatin changes, DNA repair, and transcriptional regulation.[46] We transfected mutants of nuclear actin in TR cells and found that the transfection of NLS-ActinR62D actin (defective actin polymerization) rescued the nuclear morphology of TR cells, while the NLS-ActinWT and the NLS-ActinS14C (a mutant that recapitulates the effect of jasplakinolide) did not (Figures 7A and 7B). Interestingly, transfection of NLS-ActinR62D in TR cells also reduced the nuclear area, suggesting that nuclear actin polymerization might have a dual effect on the nuclear size and wrinkling (Figure S8). As blocking actin polymerization and PKCβ signaling recovered the normal phenotype of lamin B1, we interrogated which molecular mechanism was the primary signal controlling this nuclear change in TR cells. For this, we incubated TR cells with PMA (phorbol 12-myristate 13-acetate) to stimulate the activation of PKC and observed that PMA treatment did not abrogate the effect of latrunculin on TR cells (Figure S8). Furthermore, TR cells depleted for PKCβ or preincubated with enzastaurin and treated with jasplakinolide showed that actin stabilization overcame the recovery induced by targeting PKCβ (Figures 7C and 7D). When we inverted the order and pretreated TR cells with jasplakinolide before the addition of enzastaurin, we confirmed that actin stabilization also impaired the effect induced by PKC inhibition (Figure S8). We investigated potential interactions among lamin B1, PKCβ, and actin in TR cells and found that TR cells exhibit increased levels of PKCβ associated with both actin and lamin B1 compared to control cells (Figure 7E), suggesting that interactions between PKCβ, actin, and lamin B1 may contribute to the observed alterations in nuclear architecture of TR cells. Taken together, these results insinuate that nuclear actin polymerization might contribute to the nuclear wrinkling observed in TR cells, and this effect might operate downstream of PKC signaling. Although our data demonstrate increased interactions among PKCβ, actin, and lamin B1 in TR cells, we cannot exclude the possibility that cytoplasmic actin or changes in global actin polymerization also contribute to these effects.

Cells derived after 3D mechanoadaptation present different biophysical properties and mechanical homogeneity in the nucleus

Since the nuclear size and morphology of TR cells were affected and the nuclear deformability is a critical factor of cancer cell migration,[7,8] we hypothesized that the mechanical response of the nucleus would be disturbed, contributing to changes observed *in vivo* dissemination of TR cells. To determine how the nucleus deforms upon external forces, we used a cell confiner device to induce nuclear deformation by global compression. We found that isolated nuclei from TR cells increased their nuclear deformability compared to isolated nuclei from control cells (Figures 8A and 8B). Similar changes in the nuclear deformability were observed in intact control and TR cells (Figure S9), indicating that persistent cell confinement indeed may affect the mechanical response of the nucleus. Chromatin compaction also contributes to the mechanical properties of the nucleus[5]; therefore, we first interrogated whether TR cells alter their chromatin organization. To this end, we assessed DNase I sensitivity to determine the global chromatin compaction of control and TR cells. TR cells exhibited more sensitivity to DNA digestion than control cells, suggesting a more relaxed chromatin compaction state (Figures 8C and 8D). To further explore this possibility, we treated control and TR cells with trichostatin A (TSA), a chemical drug to induce chromatin decompaction. TSA treatment significantly increased the nuclear size of control cells, while TR cells were less sensitive, indicative of a lower level of chromatin compaction than control cells (Figure S9).

To investigate these chromatin changes, we used STORM (stochastic optical reconstruction microscopy) to observe the spatial organization and density of chromatin within isolated nuclei. The qualitative analysis showed that control nuclei exhibited very low levels of chromatin density/clustering, whereas nuclei from TR cells displayed a higher density of chromatin clusters. By using SIM (structured illumination microscopy) imaging on intact control and TR cells, we found that control nuclei present a high density of chromatin distributed around the periphery of the nucleus, while nuclei from TR cells showed a more homogeneous chromatin distribution, including dense domains throughout the nucleus, consistent with the STORM measurements (Figure S10). Osmotic stress has been used to determine the mechanical response of the nucleus,[36] as swelling conditions might affect the chromatin compaction and the water diffusivity inside the nucleus. We added KCl or EDTA to isolated nuclei from control and TR cells to determine how the nucleus might respond to swelling conditions. We observed that both treatments increased the area of isolated nuclei from control and TR cells. To address whether actin polymerization might influence these differences, we treated TR cells with latrunculin and found that these isolated nuclei showed nuclear swelling similar to control cells (Figure S10). We also confirmed that latrunculin treatment reduced the chromatin sensitivity of TR cells to DNase I treatment (Figure S10).

(E) Heatmap shows the relative gene expression patterns of transcriptomics generated from control cells in suspension or embedded in 3D collagen gels ($n = 3$), reflecting log2 normalized gene expression values. The color scale illustrates the relative expression level of genes across all samples from a red color (higher expression) to a blue color (lower expression).

(F) Control or TR cells were seeded on poly-L-lysine-coated slides and incubated with 5-ethynyl uridine (EU) before fixation. Then, cells were stained with specific antibodies for EU and RNA Pol II. Bar: 10 μm.

(G) Signal intensity of EU and RNA Pol II in control and TR cells in (F). Each point represents a single cell, color coded by experimental replicate. Big dots show the mean value per experiment, and their size is proportional to the n of the corresponding experiment. $n = 4–5$ replicates, $N = 84–99$ cells ± SD.

(H) Control or TR cells were seeded on poly-L-lysine-coated slides, fixed, and stained with specific antibodies for p-RNA Pol II. Bar: 10 μm.

(I) Signal intensity of p-RNA Pol II in control and TR cells in (H). Each point represents a single cell, color coded by experimental replicate. Big dots show the mean value per experiment, and their size is proportional to the n of the corresponding experiment. $n = 3$ replicates, $N = 64–69$ cells ± SD. ***$p < 0.001$.

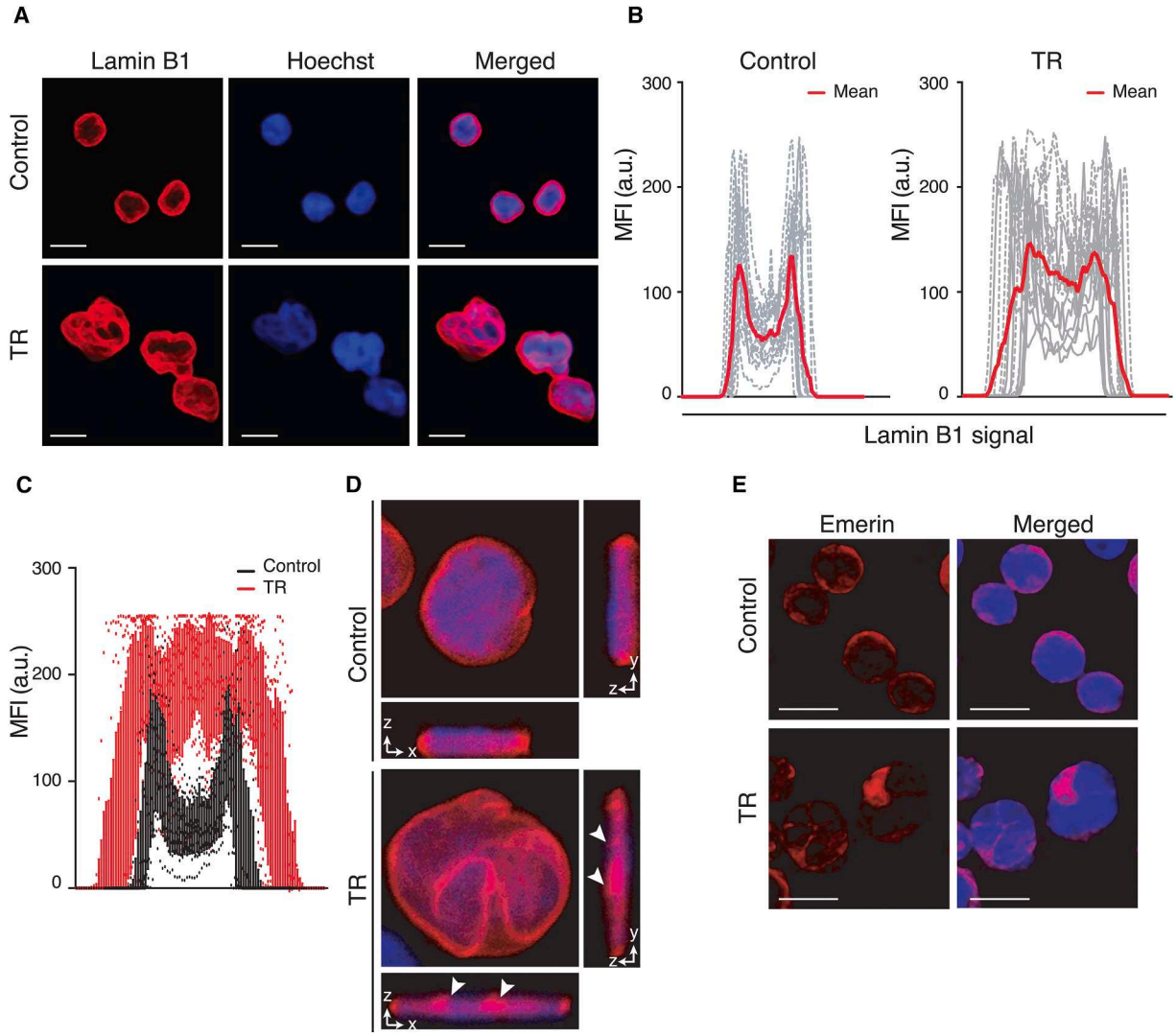

Figure 5. TR cells present multilobular nuclei characterized by an aberrant distribution of lamin B1

(A) Control or TR cells were seeded on poly-L-lysine-coated glass and stained with Hoechst (blue) and anti-lamin B1 antibody (red) for their analysis by confocal microscopy. Bar: 10 μm.

(B) Line plots show the signal (MFI [mean fluorescence intensity]) profile of lamin B1 for longitudinal sections from 15 representative cells from (A). The red line indicates the mean intensity of the profiles analyzed.

(C) Comparison between both populations (control and TR cells) for lamin B1 staining, resulting in a distinctive distribution of the signal intensity of their nuclei that resembles our previous observation.

(D) Representative middle cross-section planes of control and TR cells stained as in (A). White arrows in orthogonal views indicate lamin B1 invaginations.

(E) Control or TR cells were seeded on poly-L-lysine-coated glass and stained with Hoechst (blue) and anti-emerin antibody (red) for their analysis by confocal microscopy. Bar: 10 μm.

We have developed a methodology based on gentle poroelastic indentation using optical tweezers to apply a range of indentation depths in both isolated nuclei from control and TR cells. We determined the spatial variation of the nuclear local density (compaction, Φ) at the nuclear periphery and found an exponential decay defined by a shape factor of the function, named characteristic length ξ (Figure 8E). We found no significant differences in ξ between isolated nuclei from control and TR cells (Figure S10); nonetheless, those values from TR cells showed larger dispersion (Figure 8E), suggesting that the compaction gradient at the nuclear periphery is more heterogeneous in TR cells. To further characterize the spatial biomechanical signature of TR cells, we used AFM on isolated nuclei. Using PeakForce Capture and PeakForce Tapping, we can gain a force curve for each pixel (Figure 8F); therefore, we can measure the spatial biomechanical properties. We found that control nuclei are an inhomogeneous material with distinct high-stiffness regions (>10 kPa) and extensive softer territories (<1 kPa), while TR nuclei display a homogeneous stiffness across the nucleus (<10 kPa) (Figure 8G). To further statistically quantify these

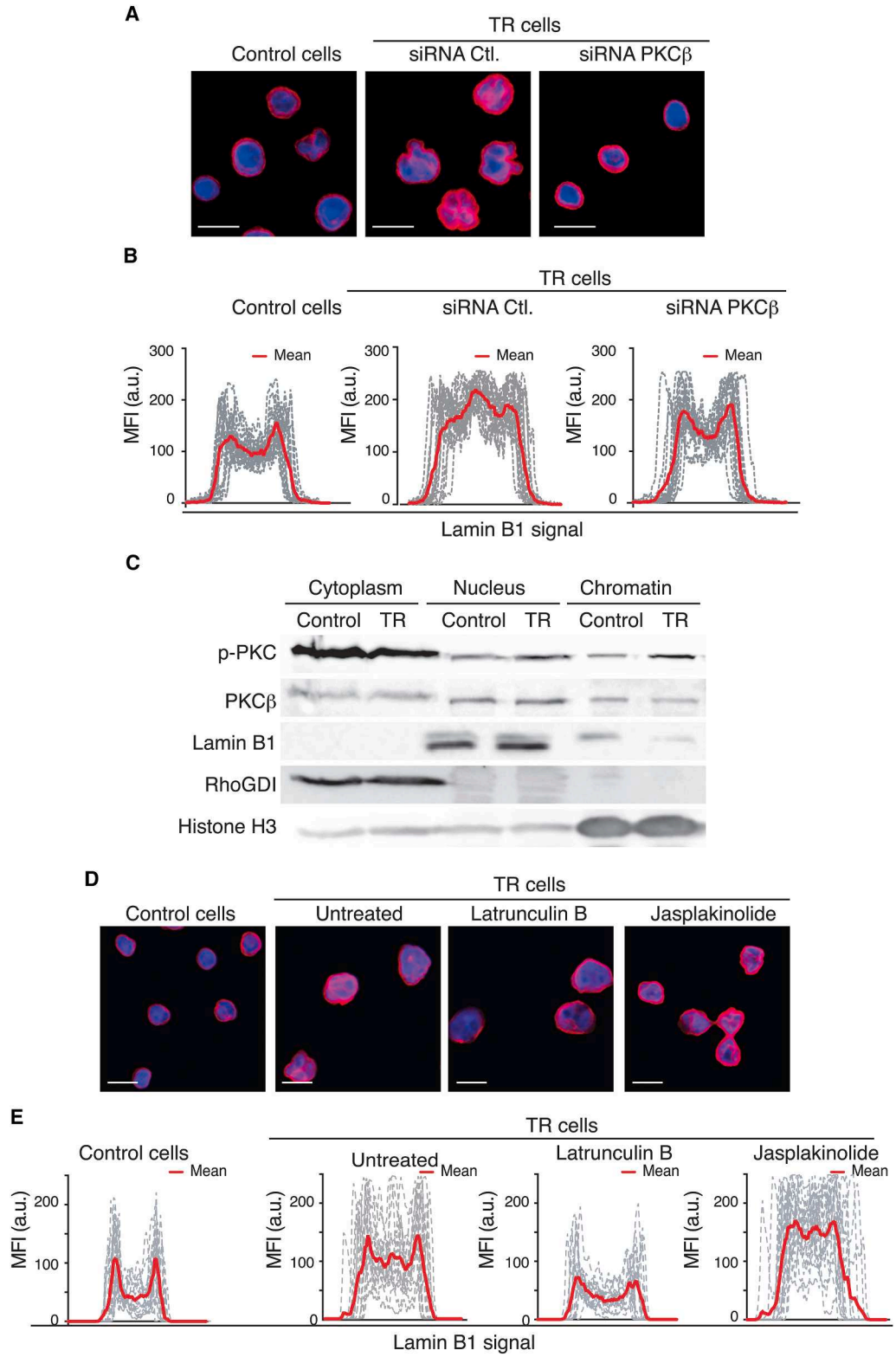

Figure 6. Persistent 3D cell confinement induces PKC-dependent redistribution of lamin B1 in TR cells

(A) TR cells were transfected with siRNA control or against PKCβ for 24 h. Then, cells were seeded on poly-L-lysine-coated glass and stained with Hoechst (blue) and anti-lamin B1 antibody (red) for their analysis by confocal microscopy. Bar: 10 μm.

(legend continued on next page)

differences, we calculated the standard deviation (SD) of the Young's modulus within individual nuclei. This analysis revealed that nuclei from control cells exhibit a higher SD compared to nuclei from TR cells, indicating greater spatial heterogeneity in nuclear stiffness (Figure 8H). In this manner, the underlying alterations within the TR cells correlated with a change in the mechanical properties. Calculating the mean stiffness for the nuclei reveals an increase in stiffness within the TR nuclei due to the loss of the distinct high- and low-stiffness domains (Figure 8I). The change in stiffness was consistent with a redistribution of lamina and chromatin, which are significant contributing factors to nuclear mechanics. Taken together, our findings indicate that TR cells showed global changes in chromatin compaction and the biomechanical signature of the nucleus.

DISCUSSION

The ECM and external stimuli play a pivotal role in regulating cell behavior by providing mechanical and biochemical signals that influence cellular transformation, senescence, metabolism, and tumor heterogeneity. Cells navigating across these constricted conditions suffer mechanical stress that promotes temporary changes in the cell nucleus, including mechanical and transcriptional alterations, nuclear blebs at the leading edge, or even the rupture of the nucleus.[47–52] However, how highly confining 3D conditions promote persistent changes in the nucleus of the cell is not fully understood. We have isolated a survivor population of Jurkat cells following confinement stress in high-density collagen gels that could be grown and expanded in suspension as TR cells. Leukocytes and leukemia cells embedded in 3D environments navigate in an amoeboid form, aligning with an integrin-independent migration.[53] Furthermore, it has been extensively reported that 3D confinement promotes an amoeboid phenotype with low adhesiveness of various cell types.[54–57] While Jurkat cells serve as a widely used model for leukemia and T lymphocyte biology, cellular responses can differ significantly across cell types in 3D culture conditions, and future investigations should evaluate the generalizability of our results in other cell types and physiological context.

As mechanical stress controls the transcriptional activity of the cell[58,59] and confined migration through narrow spaces might advantage both the selection and induction of phenotypical changes, similar to the metastatic process,[60] we focused on the transcriptional profile of TR cells. Our results cannot exclude the possibility that the persistent changes observed in TR cells result from the selection of a specific subpopulation rather than mechanoadaptation or transformation at the single-cell level. Our observations suggested that TR cells present an upregulation in their transcriptional activity, concomitant with higher levels of phospho-RNA Pol II and nucleolin. This aligns with recent evidence that demonstrates how the cell growth of human fibroblasts on geometric constraints alters their transcriptional program and induces cell-fate transitions.[37,61] Our results also align with the concept of mechanical memory, which has been defined as the potential of the ECM to imprint changes in cancer cells to metastasize from the primary tumor.[62–65] Differences compared to previous works might be due to the effects of confinement and the general influence of a 3D culture environment. Our study specifically focused on nuclear and mechanical adaptations to dense 3D matrices to model the highly confining conditions; nonetheless, we cannot discard whether a less confining 3D matrix or other mechanical compression would elicit similar responses. Interestingly, TR cells altered molecular pathways related to metabolism, cytokine signaling, and ECM remodeling. These changes indicate how mechanical stress might control metabolic pathways of migrating cells, according to previous work that highlights the role of 3D ECM stiffness on cell metabolism.[21,22] This aligns with recent studies that indicate how the ECM stiffness induces genetic variation of cancer cells and might impact human therapies.[23,66,67] These differences reinforce the idea that mechanical forces and external stimuli such as chemokines or growth factors can drive adaptive responses, such as mechanomemory, that enable cells to thrive in dynamic microenvironments. These interactions contribute to tumor heterogeneity by fostering diverse genetic and phenotypic changes, which in turn fuel cancer progression. As we have previously demonstrated that the mechanical inputs of the ECM in 3D confinement promote epigenetic and biophysical changes in normal lymphocytes and leukemia cells within 1 h,[18,68] we studied how short timescales in 3D confinement or TR cells might present similarities in their transcriptional profile. Interestingly, when we compared the transcriptional changes, we found that short or long periods of mechanical inputs generated different acute responses or long-term adaptations. Some common genes identified are critical for tumorigenesis, cellular senescence, and chromatin changes, but most transcriptional changes of TR cells indicate that the mechanical input received by cells from the ECM differs between the mechanoresponse and mechanoadaptation or memory. This aligns with the idea that the ECM dynamically interacts with cells, with effects varying depending on the duration of stimuli.[17]

We found that TR cells presented nuclear envelope wrinkling. It has been described that nuclear wrinkling is associated with multiple biological processes such as nuclear positioning, chromatin dynamics, and nuclear pore function.[69,70] Our results confirm the idea that nuclear wrinkling might be a good predictor of mechanical stress, especially for cells in 3D constraints, which generates physical stress and demands a highly dynamic nuclear envelope. Aligning with this, it has been demonstrated that breast carcinoma cells cultured on nanopillars alter their

(B) Line plots show the signal profile of lamin B1 for longitudinal sections from 15 representative cells (D). The red line indicates the mean intensity of the profiles analyzed.

(C) Control and TR cells were lysed, and the cytoplasmic, nuclear, and chromatin-bound fractions were resolved by immunoblot. Lamin B1, histone 3, and RhoGDI were used as internal controls for fractionation.

(D) TR cells were in the presence and absence of 2 μg/mL latrunculin B (an inhibitor of actin polymerization) or 1 μg/mL jasplakinolide (an actin polymerization stabilizer) for 1 h. Then, cells were seeded on poly-L-lysine-coated glass and stained with Hoechst (blue) and anti-lamin B1 antibody (red) for their analysis by confocal microscopy. Bar: 10 μm.

(E) Line plots show the signal profile of lamin B1 from 15 representative cells from (D). The red line indicates the mean intensity of the profiles analyzed.

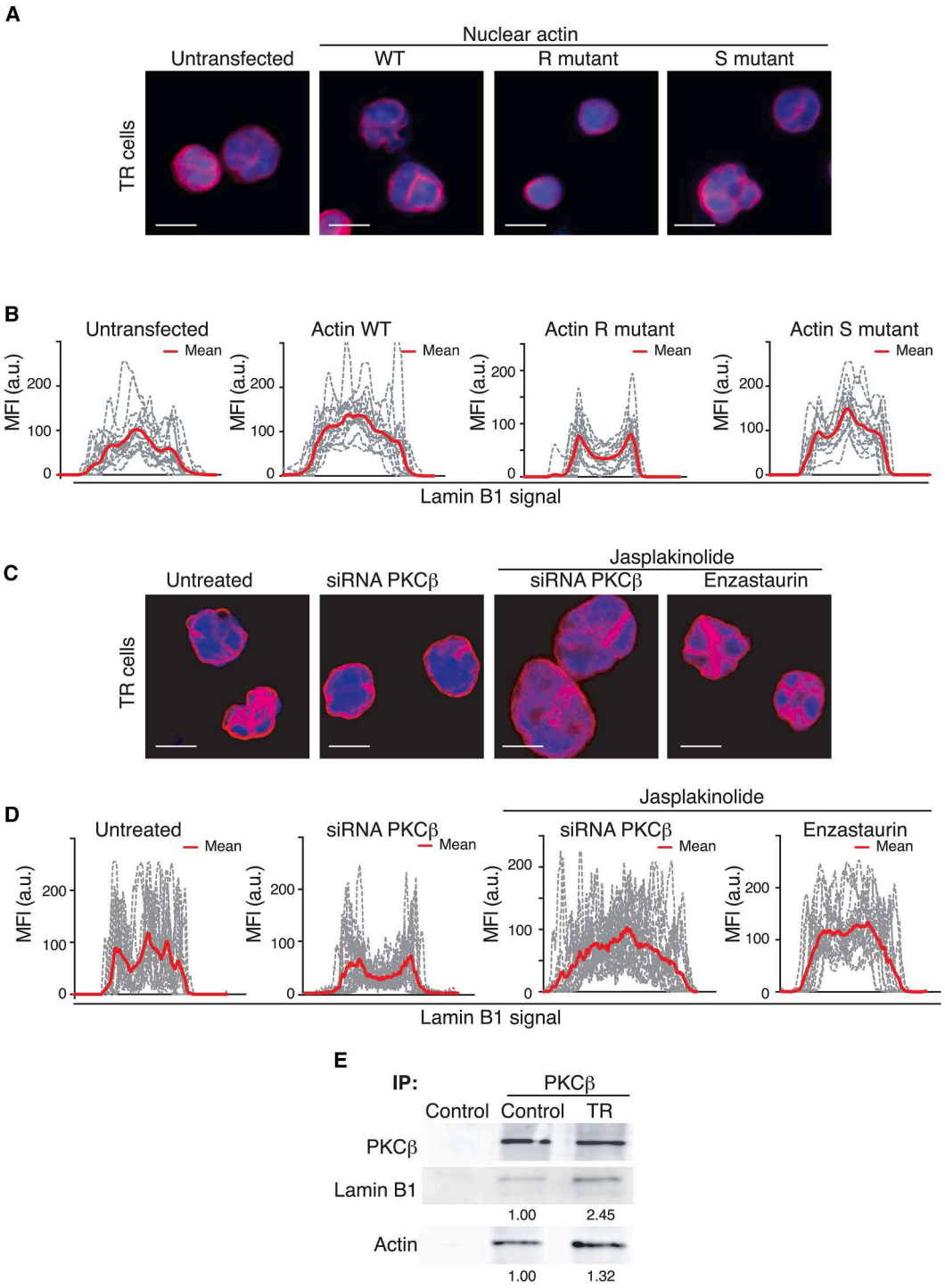

Figure 7. Nuclear actin polymerization modulates the aberrant distribution of lamin B1 in TR cells

(A) TR cells were transfected with different NLS-actin mutants for 48 h: NLS-YFP-WT (wild-type actin), NLS-YFP-R62D (R actin to impair actin polymerization), and NLS-YFP-S14C (S actin to favor actin polymerization). Cells were seeded on poly-L-lysine-coated glass and stained with Hoechst and anti-lamin B1 antibody (red) for their analysis by high-content microscopy. Bar: 10 μm.

(B) Line plots show the signal profile of lamin B1 from 15 representative cells from (A). The red line indicates the mean intensity of the profiles analyzed.

(legend continued on next page)

subnuclear morphologies and the distribution of lamin A, concomitant with higher malignancy and cell migration.[71] Visualization of lamin B1 indicates this nuclear wrinkling, in the nucleus of TR cells, rather than reflecting a distinct or functionally significant alteration in lamin B1 itself and showing a similar mechanoresilient adaptation observed in other tumor cells.[72] This also aligns with our observation that the levels of lamin B1 and other nuclear envelope markers, such as emerin and sun2, were unaltered in TR cells. We have determined that PKCβ interacts with lamin B1 and actin in TR cells. Moreover, several PKC isoforms regulate actin polymerization,[73] and we found that latrunculin treatment reduced the nuclear wrinkling in TR cells and that actin operates connected and downstream of PKC to regulate nuclear shape. This differs from a previous study, which demonstrates that the perturbation of cytoplasmic F-actin is not a major contributor to nuclear wrinkling of fruit egg chambers.[65] Using NLS-ActinR62D, we demonstrated that inhibiting nuclear actin polymerization restores normal nuclear morphology, highlighting a key role for nuclear actin in controlling nuclear envelope integrity. While cytoplasmic actin may also contribute, these findings emphasize that nuclear actomyosin is a major determinant of nuclear wrinkling, consistent with its roles in DNA repair, transcription, and cell cycle regulation.[74,75] Alterations in the nuclear size serves as a hallmark of malignancy in a broad range of cancer types, and nuclear size and volume can also be influenced by aneuploidy, osmotic stress, cytoskeletal components, and culture conditions,[76,77] with nucleolar size sometimes correlating with nuclear size.[78] Phenotypically, we also confirmed that TR cells showed an increase in the nuclear size and nucleolar signal without presenting polyploid alterations, suggesting that 3D confinement and altered actin dynamics contribute to nuclear shrinking, lateral expansion, and chromatin decompaction, emphasizing that changes in nuclear size arise from multiple, interdependent mechanisms.

Previous reports have demonstrated that the two major contributors to the DNA repair and DDR pathways, ATM and ATR, have been involved in the nuclear mechanics and lamin disposition during cancer cell migration.[79–81] Our functional characterization of TR cells showed a reduction in their invasion capacity *in vivo*, and more DNA damage markers signal in resting conditions, suggesting that these cells might suffer higher genomic stress and a predisposition to become more sensitive to specific treatments. On the other hand, our observations also align with previous work demonstrating that nuclear actin polymerization controls cellular proliferation and migration,[82] suggesting that nuclear actin homeostasis, regulated by dense 3D confinement, might present additional roles in controlling functional changes observed in TR cells. This effect on cell migration might suggest that the physical constraints of the ECM *in vivo* lead to reduced invasive capacity of cancer cells, as it has been described *in vitro* for different tumor cells across microfluidic and micropatterned devices.[83] Furthermore, the ECM stiffness can regulate cell migration while affecting other cellular functions.[84] Despite the migration ability of TR cells *in vitro*, the defective migration *in vivo* suggests difficulties colonizing other tissues in response to other tumor environmental factors while presenting higher nuclear damage caused by the mechanical stress.

This homing of leukemia cells into recipient mice is a complex process; therefore, nuclear adaptation induced by 3D confinement might have a significant dual impact on cancer cell biology by reducing cancer cell invasion and enhancing genomic instability.[85] Preventing chromatin changes resulted in impaired migration of multiple cell types through confined conditions.[35,36] Although H3K9 and DNA methylation are relevant during cell reprogramming induced by transient nuclear deformation,[80] we did not observe consistent changes of histone methylation in TR cells, even when the expression of the H3K9 methyltransferase EHMT2 is downregulated in TR cells. Aligning with this result, it has been previously reported that the epigenetic changes observed in microfluidic devices might not occur in 3D collagen matrices.[35] Chromatin compacts in a gradient extending from the nuclear lamina toward the inner nuclear regions[86,87]; however, we found that TR cells showed less compacted chromatin, leading to increased DNase I sensitivity, and redistributed around the nucleus in a similar manner to the visualization of lamin B1. Moreover, visualization of chromatin compaction by STORM in the TR cells showed alterations in the chromatin organization compared to control conditions. Our results might be connecting chromatin compaction and actin polymerization, as latrunculin treatment recovered the normal chromatin openness in TR cells; nonetheless, the specific molecular pathway responsible for the observed chromatin conformation still remains unclear. It is plausible that the less condensed chromatin of TR cells might be a key factor in regulating changes in the mechanical signature of the nucleus. First, we observed by optical tweezers that the abnormal lamin distribution found in TR cells might be linked to a more heterogeneous chromatin compaction at the nuclear periphery. Thus, we expected that control nuclei presented a more compact and homogeneous periphery while regions with a weakened surface tension can rise to nuclear wrinkling in TR cells. Furthermore, as AFM could reveal the biomechanical signature in single nuclei,[88] we further characterize changes in the biophysical signature of isolated nuclei from TR cells. This implies that the differences between the nuclear compression, AFM, and optical tweezers might be likely due to more complex factors contributing to the mechanical response of the nucleus, including a higher level of chromatin decondensation, diminution of actin polymerization, and loosening of the nuclear lamina. While differences in the influence of mechanical stress on the biophysical response of the nucleus remain open for further studies in the future, this study provides innovative insights into how TR cells mechanoadapt their nucleus through highly confining 3D environments. Together, our findings highlight the impact of cell confinement on nuclear dynamics, suggesting its

(C) TR cells were subjected to PKCβ silencing for 24 h or inhibition with 2 nM enzastaurin for 30 min, prior to treatment with 1 μg/mL jasplakinolide for an additional hour. Then, cells were seeded on poly-L-lysine-coated glass and stained with Hoechst and anti-lamin B1. Bar: 10 μm.

(D) Line plots show the signal profile of lamin B1 from 15 representative cells from (D). The red line indicates the mean intensity of the profiles analyzed.

(E) Control and TR cells were lysed, sonicated, and immunoprecipitated with anti-PKCβ antibody. The interactions with lamin B1 and actin were resolved by immunoblot. Numbers represent the protein quantification ratio after normalizing control cell values to 1.

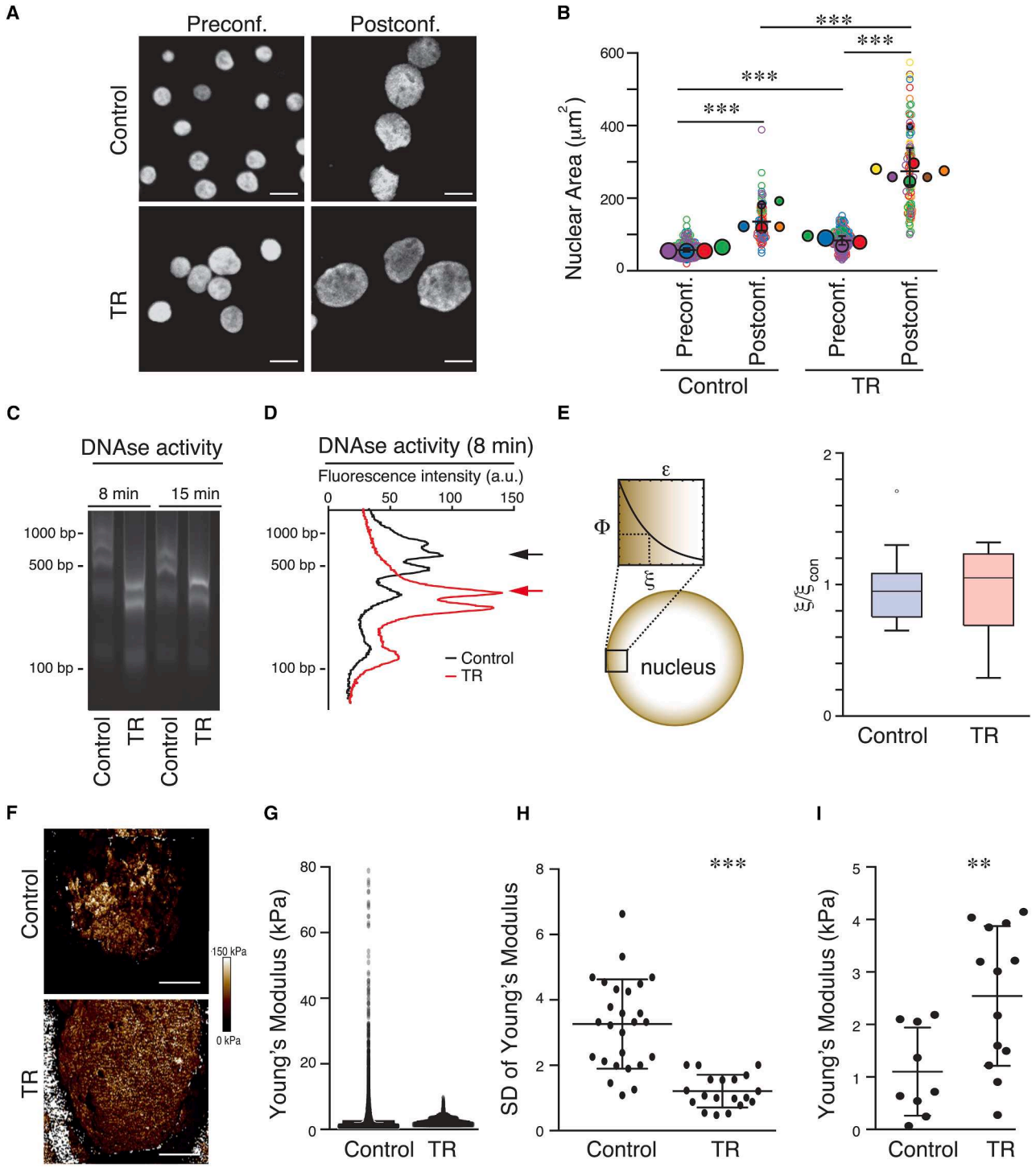

Figure 8. Persistent 3D confinement modulates nuclear biophysics and homogeneity

(A) Isolated nuclei from control and TR cells were seeded on poly-L-lysine-coated slides, stained with Hoechst, and confined mechanically up to 3 μm. Confocal images pre- and post-confinement are shown. Bar: 10 μm.

(B) Quantification of nuclear area pre- and post-confinement from (A). Each point represents a single cell, color coded by experimental replicate. Big dots show the mean value per experiment, and their size is proportional to the *n* of the corresponding experiment. *n* = 4–7 replicates, *N* = 66–227 cells ± SD.

(C) Control and TR cells were collected, and their DNA was digested with DNase I for 8 or 15 min. Then chromatin degradation was resolved in an agarose gel.

(D) DNA fragmentation profile from control (black) and TR (red) cells as in (D). Arrows indicate the maximum peak of the signal in both populations.

(legend continued on next page)

fundamental role in regulating cellular functions such as migration, transcription, and DNA repair.

Overall, our findings describe how 3D cell culture conditions alter the nuclear morphology, chromatin conformation, and the biomechanical response of the nucleus. Considering the functional changes observed in gene expression, the adaptive cell survival to drugs, and the *in vivo* migration of TR cells, our observations may contribute to explaining unknown biomechanical effects of high-density 3D collagen matrices in the nuclear biology that might occur during cancer cell invasion, tissue repair, and developmental processes. Together, this study suggests that specific mechanical conditions, induced by 3D matrices, in leukemia cells can potentially drive leukemia progression and heterogeneity and chromatin instability of survivor cells. Due to the exclusive use of leukemia cells and the specific use of high-density 3D collagen matrix conditions in this study, an extensive validation of these mechanoregulatory principles to adherent cell types will be essential to establish broader biological relevance.

METHODS

Cell culture

The human Jurkat (CVCL_0367) cell line was from the ATCC (American Type Culture Collection). Jurkat cells were cultured in complete medium (RPMI 1640 medium with L-glutamine, 25 mM HEPES [Sigma], and 10% fetal bovine serum [Sigma]) and maintained in 5% CO_2 and 37°C. TR cells were obtained upon long-term 3D confinement. For this, Jurkat cells were embedded in a solution of 3.3 mg/mL of bovine collagen type I (Stem Cell) in complete medium and neutralized with 7.5% NaHCO3 and 25 mM HEPES. After 1 h at 37°C, additional complete medium was added at the top of the 3D collagen matrix. Jurkat cells were maintained in the 3D matrix for 10 days, and the complete medium was changed every 3–4 days. Then, cells were collected from the collagen gel, cultured in suspension, and expanded as TR cells. TR cells in culture were stained to confirm persistent nuclear changes every 2 weeks.

Immunofluorescence

Cells (control and TR cells) cultured in suspension were treated or not with specific inhibitors at 37°C. Then, cells were seeded onto 10 μg/mL poly-L-lysine-coated glass slides for 30 min, fixed with 4% formaldehyde for 10 min, and permeabilized with 0.5% Triton X-100 (Tx-100) in PBS for 5 min. After 30 min blocking in 10% fetal bovine serum with 0.1% Tx-100 in PBS, samples were incubated with appropriate primary antibodies (1:100) for 1 h at room temperature (RT), followed by several PBS washes and 1 h at RT incubation with secondary antibodies (1:200). Samples were stained with 1 μg/mL Hoechst 33342 for 10 min at RT, washed with PBS and water, and mounted. Images were acquired on an inverted DMi8 microscope (Leica) using an ACS-APO 63x NA 1.30 glycerol immersion objective. Hoechst 33342 staining was acquired with the specific purpose to visualize the nucleus. Quantification and analysis of images were determined using ImageJ (National Institute of Health). 3D reconstructions and videos were obtained using Leica software. For distribution analyses, the lamin B1 signal from a cross-sectional plane of the cells was plotted, and the mean of 15 cells was calculated and marked in red.

Nuclear isolation

Nuclei were isolated by resuspending cells in buffer A (10 mM HEPES, 10 mM KCl, 1.5 mM $MgCl_2$, 0.34 M sucrose, 10% (v/v) glycerol, 1 mM DTT, 0.1% Tx100, and Roche protease inhibitor) for 5 min on ice. Following 3,800 rpm centrifugation for 5 min, the pellet with the nuclei was resuspended in TKMC buffer (50 mM Tris [pH 7.5], 25 mM KCl, 3 mM $MgCl_2$, 3 mM $CaCl_2$, and proteinase inhibitors) or PBS for conducting the indicated experiments.

AFM

AFM measurements were performed with a Bruker Bioscope Resolve mounted on an inverted microscope (Nikon Eclipse Ti2) connected to an ORCA-Flash4.0LT (Hamamatsu) camera. 8×10^5 isolated nuclei from control and TR cells were seeded on 50 mm cell culture dishes (Willco GWST-5040) coated with 100 μg/mL poly-L-lysine following the protocol in Raab et al.[19] and Denais et al.[20] Imaging was performed in filtered PBS at RT. Pre-calibrated silicon tip-nitride cantilevers (PFQNM-LC-V2 Bruker) were used with a 70 nm tip radius. PeakForce Tapping/PeakForce Capture with a maximum indentation force of 0.5 nN was used. Indentation curves were fitted within Nanoscope Analysis (Bruker) using a cone-sphere model.[21]

Mechanical compression

Complete cells or isolated nuclei from cells were resuspended in PBS, dyed with 1 μg/mL Hoechst 33342, and sedimented onto 10 μg/mL poly-L-lysine-coated plates and placed in the cell confiner device (4D cell). Following the manufacturer's instructions, mechanical confinement was performed by pushing the nuclei with a glass slide with micropillars of 3 μm height. Images of at least 20 nuclei were taken with a 63× objective before and after the confinement by an inverted confocal DMi8 microscope (Leica), and analysis of the nuclear area was performed with ImageJ.

Nuclear swelling stress

Isolated nuclei were resuspended in TKMC buffer and sedimented onto poly-L-lysine-coated plates. Nuclei were incubated or not with 5 mM EDTA or KCl for 10 min. Then, nuclei were fixed, permeabilized, and stained with Hoechst 33342 (1 μg/mL).

(E) Image on the left shows the compaction analysis based on indentation assays of isolated nuclei from control and TR cells performed with optical tweezers. The compaction parameter, Φ, decays exponentially with the indentation depth (shown here in terms of strain, ε, being R the indenter radius). The characteristic length ξ defines the compaction decay. The right graph shows the values for the isolated nuclei from control and TR expressed as the ratio.
(F) Isolated nuclei from control and TR cells were seeded on poly-L-lysine-coated dishes and imaged by AFM (atomic force microscopy). PeakForce Tapping image of a representative nucleus captured with a maximum indentation force of 0.5 nN.
(G) The graph shows the distribution of individual force curves across a single representative nucleus for each condition (>10,000 curves for each condition).
(H) Graph shows the standard deviation (SD) of the Young's modulus values for isolated nuclei from control and TR cells. N = 26–19 ± SD.
(I) Young's modulus values for isolated nuclei from control and TR cells. Each point corresponds to the average value for a nucleus, calculated from >10,000 independent force curves. N = 9–13 ± SD. $^{**}p < 0.01$ and $^{***}p < 0.001$.

Quantification and analysis of the nuclear area were determined using ImageJ software.

In vivo cell homing

NOD-SCID-Il2rg−/− (NSG) mice (*Mus musculus*) were bred and maintained at the Servicio del Animalario del Centro de Investigaciones Biológicas Margarita Salas (CIB-CSIC) with number 28079-21A. All mice were used following guidelines issued by the European and Spanish legislations for laboratory animal care. Control and TR cells were labeled with Cell Tracker Far Red (2 μM) and CFSE (5 μM), respectively, for 30 min; then, cells were mixed 1:1, and 5×10^6 mixture cells were injected intravenously (i.v.) in the tail vein of 9-week-old NSG mice. Animals were euthanized 24 h after injection, and the bone marrow from femurs, spleens, and livers was extracted, processed through mechanical disaggregation, and resuspended in erythrocyte lysis buffer (150 mM NH_4Cl, 10 mM $KHCO_3$, and 0.1 mM EDTA). Samples (1 million events) were acquired in a FacsCanto II (Beckton Dickinson) cytometer, and the percentage of labeled cells according to the total number of events in the spleen, bone marrow, and liver was analyzed using FlowJo software.

Ethics approval and consent to participate

All procedures for animal experiments were approved by the Committee on the Use and Care of Animals and carried out in strict accordance with the institution's guidelines and the European and Spanish legislations for laboratory animal care.

Statistics

The number of replicates and statistical tests used in individual experiments is specified in the figure legends. At least 2 biological replicates were performed for each experiment. Statistical analysis and comparisons were generated with GraphPad Prism 8 and IBM SPSS Statistics. The numerical data are presented as the mean ± SD. Differences between means were tested by a Student's *t* test for two-group comparisons. Where 3 or more groups were analyzed, a one-way ANOVA was performed. Individual cell measurements were color coded by experimental replicate, along with the mean value per experiment. Linear mixed models (restricted maximum likelihood estimation and variance components structure) were used to assess differences between conditions for individual cell/nuclear measurements to account for the hierarchical structure of the data. This approach allowed us to appropriately model both fixed and random effects, ensuring that the nested or grouped nature of the observations was properly considered in our analyses. SDs or standard errors of the mean (SEM) in the bar graphs are represented by error bars. Western blots were quantified using ImageJ. *p* values are indicated by asterisks ($^*p < 0.05$, $^{**}p < 0.01$, and $^{***}p < 0.001$).

RESOURCE AVAILABILITY

Lead contact

Further information and requests for resources and reagents should be directed to and will be fulfilled by the lead contact, Javier Redondo Muñoz (javier.redondo@cib.csic.es).

Materials availability

The material generated in this study will be made available upon request.

Data and code availability

- Microarray data have been deposited with the Gene Ontology Database under accession numbers GEO: GSE181375 and GSE226621 and are publicly available as of the date of publication.
- This paper does not report any original code.
- The data supporting this study are available in the manuscript and supplemental information.
- Any additional information required to reanalyze the data reported in this paper is available from the lead contact upon request.

ACKNOWLEDGMENTS

We thank the Microscopy Unit of Instituto de Investigación Biosanitaria Gregorio Marañón (IiSGM) for assistance with confocal analyses. We are also grateful to the EM and Animal Facilities of the CIB Margarita Salas platforms for their assistance and support with the EM and *in vivo* experiments and to the UCM-Genomic CAI Unit for their assistance with microarray experiments. We thank Robert Moorhead and Daniel E. Rollins for assistance and support at Royce@Sheffield. We thank Asociación Española Contra el Cáncer for support and Tobías Álvaro-Thomsen for his assistance. We wish to acknowledge the Henry Royce Institute for Advanced Materials, funded through the Engineering and Physical Sciences Research Council (EP/R00661X/1, EP/S019367/1, EP/P02470X/1, and EP/P025285/1). This research was supported by an FPI Scholarship 2018 (Ministerio de Ciencia e Innovación [MICINN], Agencia Estatal de Investigación [AEI], and Fondo Europeo de Desarrollo Regional [FEDER]) to R.G.-N.; grants from Comunidad de Madrid (Y2018/BIO-5207) and the MICINN AEI (PID2020-115444GB-I00 and AEI/10.13039/501100011033) to P.R.-N.; grants from the MICINN AEI (PID2019-108391RB-100) and Comunidad de Madrid (Y2018/BIO-5207, S2018/NMT-4389, and REACT-EU program PR38-21-28 ANTICIPA-CM) to F.M.; a Biotechnology and Biological Sciences Research Council award (BB/X008460/1), the Medical Research Council (MR/M020606/1), and the Science and Technology Facilities Council (19130001) to C.P.T.; and grants from the 2020 Leonardo Grant for Researchers and Cultural Creators (BBVA Foundation), Ayuda de contratación de ayudante de investigación PEJ-2020-AI/BMD-19152 (Comunidad de Madrid), and the MICINN AEI (PID2020-118525RB-I00, AEI/10.13039/501100011033, and PID2023-150232OB-I00) to J.R.M.

AUTHOR CONTRIBUTIONS

R.G.-N. and H.Z.-C. conducted the experiments and contributed to data interpretation and discussions. M.A. conducted the experiments and analysis. A.d.L.-P. conducted the experiments and contributed to data interpretation. H.L.-M. conducted the experiments and contributed to data interpretation. P.R.-N. and F.M. supervised the experiments related to the optical tweezers, contributed to data interpretation, and provided financing. L.W. designed and supervised the experiments related to STORM. C.P.T. designed and supervised the experiments related to STORM and AFM, contributed to data interpretation, and provided financing. J.R.M. designed and supervised the experiments, contributed to data interpretation, wrote the paper, and provided financing.

DECLARATION OF INTERESTS

The authors declare no conflicts of interest.

SUPPLEMENTAL INFORMATION

Supplemental information can be found online at https://doi.org/10.1016/j.xcrp.2026.103116.

Received: February 7, 2025
Revised: January 9, 2026
Accepted: January 13, 2026
Published: February 18, 2026

REFERENCES

1. Carollo, P.S., and Barra, V. (2023). Chromatin epigenetics and nuclear lamina keep the nucleus in shape: Examples from natural and accelerated aging. Biol. Cell *115*, e2200023.
2. Burke, B., and Stewart, C.L. (2013). The nuclear lamins: flexibility in function. Nat. Rev. Mol. Cell Biol. *14*, 13–24.
3. Cho, S., Irianto, J., and Discher, D.E. (2017). Mechanosensing by the nucleus: From pathways to scaling relationships. J. Cell Biol. *216*, 305–315.
4. Dahl, K.N., Ribeiro, A.J.S., and Lammerding, J. (2008). Nuclear shape, mechanics, and mechanotransduction. Circ. Res. *102*, 1307–1318.
5. Stephens, A.D., Banigan, E.J., Adam, S.A., Goldman, R.D., and Marko, J.F. (2017). Chromatin and lamin A determine two different mechanical response regimes of the cell nucleus. Mol. Biol. Cell *28*, 1984–1996.
6. Lammerding, J., Engler, A.J., and Kamm, R. (2022). Mechanobiology of the cell nucleus. APL Bioeng. *6*, 040401.
7. Mierke, C.T. (2019). The matrix environmental and cell mechanical properties regulate cell migration and contribute to the invasive phenotype of cancer cells. Rep. Prog. Phys. *82*, 064602.
8. Jung-Garcia, Y., Maiques, O., Monger, J., Rodriguez-Hernandez, I., Fanshawe, B., Domart, M.C., Renshaw, M.J., Marti, R.M., Matias-Guiu, X., Collinson, L.M., et al. (2023). LAP1 supports nuclear adaptability during constrained melanoma cell migration and invasion. Nat. Cell Biol. *25*, 108–119.
9. Alisafaei, F., Jokhun, D.S., Shivashankar, G.V., and Shenoy, V.B. (2019). Regulation of nuclear architecture, mechanics, and nucleocytoplasmic shuttling of epigenetic factors by cell geometric constraints. Proc. Natl. Acad. Sci. USA *116*, 13200–13209.
10. Damodaran, K., Venkatachalapathy, S., Alisafaei, F., Radhakrishnan, A.V., Sharma Jokhun, D., Shenoy, V.B., and Shivashankar, G.V. (2018). Compressive force induces reversible chromatin condensation and cell geometry–dependent transcriptional response. Mol. Biol. Cell *29*, 3039–3051.
11. Guilluy, C., Osborne, L.D., Van Landeghem, L., Sharek, L., Superfine, R., Garcia-Mata, R., and Burridge, K. (2014). Isolated nuclei adapt to force and reveal a mechanotransduction pathway in the nucleus. Nat. Cell Biol. *16*, 376–381.
12. Pickup, M.W., Mouw, J.K., and Weaver, V.M. (2014). The extracellular matrix modulates the hallmarks of cancer. EMBO Rep. *15*, 1243–1253.
13. Zhong, J., Yang, Y., Liao, L., and Zhang, C. (2020). Matrix stiffness-regulated cell functions under different dimensionalities. Biomater. Sci. *8*, 2734–2755.
14. Wullkopf, L., West, A.K.V., Leijnse, N., Cox, T.R., Madsen, C.D., Oddershede, L.B., and Erler, J.T. (2018). Cancer cells' ability to mechanically adjust to extracellular matrix stiffness correlates with their invasive potential. Mol. Biol. Cell *29*, 2378–2385.
15. Urbanczyk, M., Layland, S.L., and Schenke-Layland, K. (2020). The role of extracellular matrix in biomechanics and its impact on bioengineering of cells and 3D tissues. Matrix Biol. *85–86*, 1–14.
16. Saraswathibhatla, A., Indana, D., and Chaudhuri, O. (2023). Cell-extracellular matrix mechanotransduction in 3D. Nat. Rev. Mol. Cell Biol. *24*, 495–516.
17. Engler, A.J., Sen, S., Sweeney, H.L., and Discher, D.E. (2006). Matrix elasticity directs stem cell lineage specification. Cell *126*, 677–689.
18. Wang, P., Dreger, M., Madrazo, E., Williams, C.J., Samaniego, R., Hodson, N.W., Monroy, F., Baena, E., Sánchez-Mateos, P., Hurlstone, A., and Redondo-Muñoz, J. (2018). WDR5 modulates cell motility and morphology and controls nuclear changes induced by a 3D environment. Proc. Natl. Acad. Sci. USA *115*, 8581–8586.
19. Raab, M., Gentili, M., de Belly, H., Thiam, H.R., Vargas, P., Jimenez, A.J., Lautenschlaeger, F., Voituriez, R., Lennon-Duménil, A.M., Manel, N., and Piel, M. (2016). ESCRT III repairs nuclear envelope ruptures during cell migration to limit DNA damage and cell death. Science *352*, 359–362.
20. Denais, C.M., Gilbert, R.M., Isermann, P., McGregor, A.L., te Lindert, M., Weigelin, B., Davidson, P.M., Friedl, P., Wolf, K., and Lammerding, J. (2016). Nuclear envelope rupture and repair during cancer cell migration. Science *352*, 353–358.
21. Bertolio, R., Napoletano, F., and Del Sal, G. (2023). Dynamic links between mechanical forces and metabolism shape the tumor milieu. Curr. Opin. Cell Biol. *84*, 102218.
22. Romani, P., Nirchio, N., Arboit, M., Barbieri, V., Tosi, A., Michielin, F., Shibuya, S., Benoist, T., Wu, D., Hindmarch, C.C.T., et al. (2022). Mitochondrial fission links ECM mechanotransduction to metabolic redox homeostasis and metastatic chemotherapy resistance. Nat. Cell Biol. *24*, 168–180.
23. Ilina, O., Gritsenko, P.G., Syga, S., Lippoldt, J., La Porta, C.A.M., Chepizhko, O., Grosser, S., Vullings, M., Bakker, G.J., Starruß, J., et al. (2020). Cell-cell adhesion and 3D matrix confinement determine jamming transitions in breast cancer invasion. Nat. Cell Biol. *22*, 1103–1115.
24. Cukierman, E., Pankov, R., and Yamada, K.M. (2002). Cell interactions with three-dimensional matrices. Curr. Opin. Cell Biol. *14*, 633–639.
25. Kim, J.B. (2005). Three-dimensional tissue culture models in cancer biology. Semin. Cancer Biol. *15*, 365–377.
26. Wolf, K., Te Lindert, M., Krause, M., Alexander, S., Te Riet, J., Willis, A.L., Hoffman, R.M., Figdor, C.G., Weiss, S.J., and Friedl, P. (2013). Physical limits of cell migration: control by ECM space and nuclear deformation and tuning by proteolysis and traction force. J. Cell Biol. *201*, 1069–1084.
27. Noro, J., Vilaça-Faria, H., Reis, R.L., and Pirraco, R.P. (2024). Extracellular matrix-derived materials for tissue engineering and regenerative medicine: A journey from isolation to characterization and application. Bioact. Mater. *34*, 494–519.
28. Mierke, C.T. (2024). Extracellular Matrix Cues Regulate Mechanosensing and Mechanotransduction of Cancer Cells. Cells *13*, 96.
29. Wolf, K., and Friedl, P. (2011). Extracellular matrix determinants of proteolytic and non-proteolytic cell migration. Trends Cell Biol. *21*, 736–744.
30. Radhakrishnan, A., Damodaran, K., Soylemezoglu, A.C., Uhler, C., and Shivashankar, G.V. (2017). Machine Learning for Nuclear Mechano-Morphometric Biomarkers in Cancer Diagnosis. Sci. Rep. *7*, 17946.
31. Tzur, A., Moore, J.K., Jorgensen, P., Shapiro, H.M., and Kirschner, M.W. (2011). Optimizing optical flow cytometry for cell volume-based sorting and analysis. PLoS One *6*, e16053.
32. Tilghman, R.W., Cowan, C.R., Mih, J.D., Koryakina, Y., Gioeli, D., Slack-Davis, J.K., Blackman, B.R., Tschumperlin, D.J., and Parsons, J.T. (2010). Matrix rigidity regulates cancer cell growth and cellular phenotype. PLoS One *5*, e12905.
33. Streichan, S.J., Hoerner, C.R., Schneidt, T., Holzer, D., and Hufnagel, L. (2014). Spatial constraints control cell proliferation in tissues. Proc. Natl. Acad. Sci. USA *111*, 5586–5591.
34. Cho, S., Vashisth, M., Abbas, A., Majkut, S., Vogel, K., Xia, Y., Ivanovska, I.L., Irianto, J., Tewari, M., Zhu, K., et al. (2019). Mechanosensing by the Lamina Protects against Nuclear Rupture, DNA Damage, and Cell-Cycle Arrest. Dev. Cell *49*, 920–935.e5.
35. Hsia, C.R., McAllister, J., Hasan, O., Judd, J., Lee, S., Agrawal, R., Chang, C.Y., Soloway, P., and Lammerding, J. (2022). Confined migration induces heterochromatin formation and alters chromatin accessibility. iScience *25*, 104978.
36. Zhang, X., Cook, P.C., Zindy, E., Williams, C.J., Jowitt, T.A., Streuli, C.H., MacDonald, A.S., and Redondo-Muñoz, J. (2016). Integrin a4b1 controls G9a activity that regulates epigenetic changes and nuclear properties required for lymphocyte migration. Nucleic Acids Res. *44*, 3031–3044.
37. Roy, B., Yuan, L., Lee, Y., Bharti, A., Mitra, A., and Shivashankar, G.V. (2020). Fibroblast rejuvenation by mechanical reprogramming and redifferentiation. Proc. Natl. Acad. Sci. USA *117*, 10131–10141.
38. Poulard, C., Baulu, E., Lee, B.H., Pufall, M.A., and Stallcup, M.R. (2018). Increasing G9a automethylation sensitizes B acute lymphoblastic leukemia cells to glucocorticoid-induced death. Cell Death Dis. *9*, 1038.
39. Madrazo, E., Ruano, D., Abad, L., Alonso-Gómez, E., Sánchez-Valdepeñas, C., González-Murillo, Á., Ramírez, M., and Redondo-Muñoz, J.

(2018). G9a Correlates with VLA-4 Integrin and Influences the Migration of Childhood Acute Lymphoblastic Leukemia Cells. Cancers *10*, 325.

40. Röber, R.A., Sauter, H., Weber, K., and Osborn, M. (1990). Cells of the cellular immune and hemopoietic system of the mouse lack lamins A/C: distinction versus other somatic cells. J. Cell Sci. *95*, 587–598.
41. Sen Gupta, A., and Sengupta, K. (2017). Lamin B2 Modulates Nucleolar Morphology, Dynamics, and Function. Mol. Cell Biol. *37*, e00274-17.
42. Martin, C., Chen, S., Maya-Mendoza, A., Lovric, J., Sims, P.F.G., and Jackson, D.A. (2009). Lamin B1 maintains the functional plasticity of nucleoli. J. Cell Sci. *122*, 1551–1562.
43. Tang, C.W., Maya-Mendoza, A., Martin, C., Zeng, K., Chen, S., Feret, D., Wilson, S.A., and Jackson, D.A. (2008). The integrity of a lamin-B1-dependent nucleoskeleton is a fundamental determinant of RNA synthesis in human cells. J. Cell Sci. *121*, 1014–1024.
44. Torvaldson, E., Kochin, V., and Eriksson, J.E. (2015). Phosphorylation of lamins determine their structural properties and signaling functions. Nucleus *6*, 166–171.
45. Yamazaki, D., Kurisu, S., and Takenawa, T. (2005). Regulation of cancer cell motility through actin reorganization. Cancer Sci. *96*, 379–386.
46. de Lanerolle, P. (2012). Nuclear actin and myosins at a glance. J. Cell Sci. *125*, 4945–4949.
47. van Helvert, S., Storm, C., and Friedl, P. (2018). Mechanoreciprocity in cell migration. Nat. Cell Biol. *20*, 8–20.
48. Graziani, V., Crosas-Molist, E., George, S.L., and Sanz-Moreno, V. (2024). Organelle adaptations in response to mechanical forces during tumour dissemination. Curr. Opin. Cell Biol. *88*, 102345.
49. Kalukula, Y., Stephens, A.D., Lammerding, J., and Gabriele, S. (2022). Mechanics and functional consequences of nuclear deformations. Nat. Rev. Mol. Cell Biol. *23*, 583–602.
50. Shah, P., Hobson, C.M., Cheng, S., Colville, M.J., Paszek, M.J., Superfine, R., and Lammerding, J. (2021). Nuclear deformation causes DNA damage by increasing replication stress. Curr. Biol. *31*, 753–765.e6.
51. Irianto, J., Xia, Y., Pfeifer, C.R., Athirasala, A., Ji, J., Alvey, C., Tewari, M., Bennett, R.R., Harding, S.M., Liu, A.J., et al. (2017). DNA damage follows repair factor depletion and portends genome variation in cancer cells after pore migration. Curr. Biol. *27*, 210–223.
52. Lämmermann, T., Bader, B.L., Monkley, S.J., Worbs, T., Wedlich-Söldner, R., Hirsch, K., Keller, M., Förster, R., Critchley, D.R., Fässler, R., and Sixt, M. (2008). Rapid leukocyte migration by integrin-independent flowing and squeezing. Nature *453*, 51–55.
53. Liu, Y.J., Le Berre, M., Lautenschlaeger, F., Maiuri, P., Callan-Jones, A., Heuzé, M., Takaki, T., Voituriez, R., and Piel, M. (2015). Confinement and low adhesion induce fast amoeboid migration of slow mesenchymal cells. Cell *160*, 659–672.
54. Panková, K., Rösel, D., Novotný, M., and Brábek, J. (2010). The molecular mechanisms of transition between mesenchymal and amoeboid invasiveness in tumor cells. Cell. Mol. Life Sci. *67*, 63–71.
55. Graziani, V., Rodriguez-Hernandez, I., Maiques, O., and Sanz-Moreno, V. (2022). The amoeboid state as part of the epithelial-to-mesenchymal transition programme. Trends Cell Biol. *32*, 228–242.
56. Tajik, A., Zhang, Y., Wei, F., Sun, J., Jia, Q., Zhou, W., Singh, R., Khanna, N., Belmont, A.S., and Wang, N. (2016). Transcription upregulation via force-induced direct stretching of chromatin. Nat. Mater. *15*, 1287–1296.
57. Stowers, R.S., Shcherbina, A., Israeli, J., Gruber, J.J., Chang, J., Nam, S., Rabiee, A., Teruel, M.N., Snyder, M.P., Kundaje, A., and Chaudhuri, O. (2019). Matrix stiffness induces a tumorigenic phenotype in mammary epithelium through changes in chromatin accessibility. Nat. Biomed. Eng. *3*, 1009–1019.
58. Golloshi, R., Playter, C., Freeman, T.F., Das, P., Raines, T.I., Garretson, J.H., Thurston, D., and McCord, R.P. (2022). Constricted migration is associated with stable 3D genome structure differences in cancer cells. EMBO Rep. *23*, e52149.
59. Yuan, L., Roy, B., Ratna, P., Uhler, C., and Shivashankar, G.V. (2022). Lateral confined growth of cells activates Lef1 dependent pathways to regulate cell-state transitions. Sci. Rep. *12*, 17318.
60. Cambria, E., Coughlin, M.F., Floryan, M.A., Offeddu, G.S., Shelton, S.E., and Kamm, R.D. (2024). Linking cell mechanical memory and cancer metastasis. Nat. Rev. Cancer *24*, 216–228.
61. Yang, C., Tibbitt, M.W., Basta, L., and Anseth, K.S. (2014). Mechanical memory and dosing influence stem cell fate. Nat. Mater. *13*, 645–652.
62. Lee, J.W.N., and Holle, A.W. (2024). Engineering approaches for understanding mechanical memory in cancer metastasis. APL Bioeng. *8*, 021503.
63. González-Novo, R., de Lope-Planelles, A., Cruz Rodríguez, M.P., González-Murillo, Á., Madrazo, E., Acitores, D., García de Lacoba, M., Ramírez, M., and Redondo-Muñoz, J. (2023). 3D environment controls H3K4 methylation and the mechanical response of the nucleus in acute lymphoblastic leukemia cells. Eur. J. Cell Biol. *102*, 151343.
64. Cosgrove, B.D., Loebel, C., Driscoll, T.P., Tsinman, T.K., Dai, E.N., Heo, S.J., Dyment, N.A., Burdick, J.A., and Mauck, R.L. (2021). Nuclear envelope wrinkling predicts mesenchymal progenitor cell mechano-response in 2D and 3D microenvironments. Biomaterials *270*, 120662.
65. Jackson, J.A., Romeo, N., Mietke, A., Burns, K.J., Totz, J.F., Martin, A.C., Dunkel, J., and Alsous, J.I. (2023). Scaling behaviour and control of nuclear wrinkling. Nat. Phys. *19*, 1927–1935.
66. Mai, Z., Lin, Y., Lin, P., Zhao, X., and Cui, L. (2024). Modulating extracellular matrix stiffness: a strategic approach to boost cancer immunotherapy. Cell Death Dis. *15*, 307.
67. Wang, T.C., Sawhney, S., Morgan, D., Bennett, R.L., Rashmi, R., Estecio, M.R., Brock, A., Singh, I., Baer, C.F., Licht, J.D., and Lele, T.P. (2024). Genetic variation drives cancer cell adaptation to ECM stiffness. Proc. Natl. Acad. Sci. USA *121*, e2403062121.
68. Zeng, Y., Zhuang, Y., Vinod, B., Guo, X., Mitra, A., Chen, P., Saggio, I., Shivashankar, G.V., Gao, W., and Zhao, W. (2022). Guiding Irregular Nuclear Morphology on Nanopillar Arrays for Malignancy Differentiation in Tumor Cells. Nano Lett. *22*, 7724–7733.
69. Jiang, K., Lim, S.B., Xiao, J., Jokhun, D.S., Shang, M., Song, X., Zhang, P., Liang, L., Low, B.C., Shivashankar, G.V., and Lim, C.T. (2023). Deleterious Mechanical Deformation Selects Mechanoresilient Cancer Cells with Enhanced Proliferation and Chemoresistance. Adv. Sci. *10*, e2201663.
70. Lammerding, J., Fong, L.G., Ji, J.Y., Reue, K., Stewart, C.L., Young, S.G., and Lee, R.T. (2006). Lamins A and C but not lamin B1 regulate nuclear mechanics. J. Biol. Chem. *281*, 25768–25780.
71. Singh, I., and Lele, T.P. (2022). Nuclear Morphological Abnormalities in Cancer: A Search for Unifying Mechanisms. Results Probl. Cell Differ. *70*, 443–467.
72. Ottaviano, Y., and Gerace, L. (1985). Phosphorylation of the nuclear lamins during interphase and mitosis. J. Biol. Chem. *260*, 624–632.
73. Iwabu, A., Smith, K., Allen, F.D., Lauffenburger, D.A., and Wells, A. (2004). Epidermal growth factor induces fibroblast contractility and motility via a protein kinase C delta-dependent pathway. J. Biol. Chem. *279*, 14551–14560.
74. Cook, A.W., and Toseland, C.P. (2021). The roles of nuclear myosin in the DNA damage response. J. Biochem. *169*, 265–271.
75. Fili, N., Hari-Gupta, Y., Dos Santos, Á., Cook, A., Poland, S., Ameer-Beg, S.M., Parsons, M., and Toseland, C.P. (2017). NDP52 activates nuclear myosin VI to enhance RNA polymerase II transcription. Nat. Commun. *8*, 1871.
76. Katiyar, A., Tocco, V.J., Li, Y., Aggarwal, V., Tamashunas, A.C., Dickinson, R.B., and Lele, T.P. (2019). Nuclear size changes caused by local motion of cell boundaries unfold the nuclear lamina and dilate chromatin and intranuclear bodies. Soft Matter *15*, 9310–9317.
77. Kim, D.H., Li, B., Si, F., Phillip, J.M., Wirtz, D., and Sun, S.X. (2015). Volume regulation and shape bifurcation in the cell nucleus. J. Cell Sci. *128*, 3375–3385.

78. Mukherjee, R.N., Chen, P., and Levy, D.L. (2016). Recent advances in understanding nuclear size and shape. Nucleus *7*, 167–186.

79. Dos Santos, Á., Cook, A.W., Gough, R.E., Schilling, M., Olszok, N.A., Brown, I., Wang, L., Aaron, J., Martin-Fernandez, M.L., Rehfeldt, F., and Toseland, C.P. (2021). DNA damage alters nuclear mechanics through chromatin reorganization. Nucleic Acids Res. *49*, 340–353.

80. Kidiyoor, G.R.,, Li, Q., Bastianello, G., Bruhn, C., Giovannetti, I., Mohamood, A., Beznoussenko, G.V., Mironov, A., Raab, M., Piel, M., et al. (2020). ATR is essential for preservation of cell mechanics and nuclear integrity during interstitial migration. Nat. Commun. *11*, 4828.

81. Shah, P., McGuigan, C.W., Cheng, S., Vanpouille-Box, C., Demaria, S., Weiss, R.S., and Lammerding, J. (2022). ATM Modulates Nuclear Mechanics by Regulating Lamin A Levels. Front. Cell Dev. Biol. *10*, 875132.

82. McNeill, M.C., Wray, J., Sala-Newby, G.B., Hindmarch, C.C.T., Smith, S.A., Ebrahimighaei, R., Newby, A.C., and Bond, M. (2020). Nuclear actin regulates cell proliferation and migration via inhibition of SRF and TEAD. Biochim. Biophys. Acta. Mol. Cell Res. *1867*, 118691.

83. Dudaryeva, O.Y., Bernhard, S., Tibbitt, M.W., and Labouesse, C. (2023). Implications of Cellular Mechanical Memory in Bioengineering. ACS Biomater. Sci. Eng. *9*, 5985–5998.

84. Song, Y., Soto, J., Chen, B., Hoffman, T., Zhao, W., Zhu, N., Peng, Q., Liu, L., Ly, C., Wong, P.K., et al. (2022). Transient nuclear deformation primes epigenetic state and promotes cell reprogramming. Nat. Mater. *21*, 1191–1199.

85. Yang, B., Wolfenson, H., Chung, V.Y., Nakazawa, N., Liu, S., Hu, J., Huang, R.Y.J., and Sheetz, M.P. (2020). Stopping transformed cancer cell growth by rigidity sensing. Nat. Mater. *19*, 239–250.

86. Dos Santos, Á., Gough, R.E., Wang, L., and Toseland, C.P. (2022). Measuring Nuclear Organization of Proteins with STORM Imaging and Cluster Analysis. Chromosome Architecture. Methods Mol. Biol. *2476*, 293–309.

87. Le Gros, M.A., Clowney, E.J., Magklara, A., Yen, A., Markenscoff-Papadimitriou, E., Colquitt, B., Myllys, M., Kellis, M., Lomvardas, S., and Larabell, C.A. (2016). Soft X-Ray tomography reveals gradual chromatin compaction and reorganization during neurogenesis in vivo. Cell Rep. *17*, 2125–2136.

88. Lherbette, M., Dos Santos, Á., Hari-Gupta, Y., Fili, N., Toseland, C.P., and Schaap, I.A.T. (2017). Atomic Force Microscopy micro-rheology reveals large structural inhomogeneities in single cell-nuclei. Sci. Rep. *7*, 8116.